ADVANCES IN ATMOSPHERIC SCIENCES, VOL. 34, NOVEMBER 2017, 1358–1379

• **Original Paper** •

Influence of the Preceding Austral Summer Southern Hemisphere Annular Mode on the Amplitude of ENSO Decay

Fei ZHENG*[1], Jianping LI[2,3], and Ruiqiang DING[1,4]

[1]*State Key Laboratory of Numerical Modeling for Atmospheric Sciences and Geophysical Fluid Dynamics, Institute of Atmospheric Physics, Chinese Academy of Sciences, Beijing* 100029*, China*

[2]*College of Global Change and Earth System Science, Beijing Normal University, Beijing* 100875*, China*

[3]*Laboratory for Regional Oceanography and Numerical Modeling, Qingdao National Laboratory for Marine Science and Technology, Qingdao* 266237*, China*

[4]*Plateau Atmosphere and Environment Key Laboratory of Sichuan Province, Chengdu University of Information Technology, Chengdu* 610103*, China*

(Received 3 January 2017; revised 1 May 2017; accepted 22 May 2017)

ABSTRACT

There is increasing evidence of the possible role of extratropical forcing in the evolution of ENSO. The Southern Hemisphere Annular Mode (SAM) is the dominant mode of atmospheric circulation in the Southern Hemisphere extratropics. This study shows that the austral summer (December–January–February; DJF) SAM may also influence the amplitude of ENSO decay during austral autumn (March–April–May; MAM). The mechanisms associated with this SAM–ENSO relationship can be briefly summarized as follows: The SAM is positively (negatively) correlated with SST in the Southern Hemisphere middle (high) latitudes. This dipole-like SST anomaly pattern is referred to as the Southern Ocean Dipole (SOD). The DJF SOD, caused by the DJF SAM, could persist until MAM and then influence atmospheric circulation, including trade winds, over the Niño3.4 area. Anomalous trade winds and SST anomalies over the Niño3.4 area related to the DJF SAM are further developed through the Bjerkness feedback, which eventually results in a cooling (warming) over the Niño3.4 area followed by the positive (negative) DJF SAM.

Key words: Southern Hemisphere Annular Mode, ENSO, Southern Ocean Dipole

Citation: Zheng, F., J. P. Li, and R. Q. Ding, 2017: Influence of the preceding austral summer Southern Hemisphere annular mode on the amplitude of ENSO decay. *Adv. Atmos. Sci.*, **34**(11), 1358–1379, https://doi.org/10.1007/s00376-017-6339-4.

1. Introduction

In the Southern Hemisphere extratropics, the dominant mode of atmospheric circulation is a large-scale oscillation referred to as the Southern Hemisphere annular mode (SAM; Hartmann and Lo, 1998; Gong and Wang, 1999; Thompson and Wallace, 2000; Li and Wang, 2003). The SAM is characterized by a seesaw pattern in sea level pressure between the middle and high southern latitudes, and is accompanied by a meridional shift of in the midlatitude westerlies. When the SAM is in a positive (negative) phase, the westerly jet shifts towards the Antarctic (tropics). The SAM is an internal atmospheric mode and is excited and maintained by the feedbacks between eddy activity and zonal mean flow (e.g., Feldstein and Lee, 1998; Lorenz and Hartmann, 2001; Luo et al., 2007; Zhang et al., 2012), and air–sea interactions may contribute to SAM variability (Watterson, 2000; Gupta and England, 2007).

The SAM is observed to vary in response to El Niño–Southern Oscillation (ENSO) during austral spring and summer. Positive (negative) SAM phases dominate during La Niña (El Niño) events. Support for the role of ENSO in shaping the SAM has been obtained from both observations (Fogt and Bromwich, 2006; L'Heureux and Thompson, 2006) and model simulations (Zhou and Yu, 2004). These studies found that tropical forcing can influence SAM variability through physical processes such as modulating Rossby wave activity. For example, Gong et al. (2010) proposed that the background zonal-mean flow related to La Niña (El Niño) is a precondition for strong (weak) anticyclonic wave breaking on the equatorward side of the eddy-driven jet, which tends to drive positive (negative) SAM events. Ding et al. (2012) pointed out that long-term changes in tropical Pacific sea surface temperature (SST) contribute to the positive trend in the SAM. Furthermore, Ciasto et al. (2015) found that SST in

* Corresponding author: Fei ZHENG
Email: zhengfei08@mail.iap.ac.cn

different regions of tropical Pacific play different role in influencing the SAM. Specifically, eastern Pacific SST variability has a strong influence on the SAM, whereas central Pacific SST has only a weak correlation with the SAM.

Given that studies have found that ENSO may modulate the SAM, it is natural to also question whether the SAM might play a role in influencing ENSO or, more generally, tropical Pacific SST. It is commonly assumed that tropical SSTs are controlled by tropical mechanisms, including the surface heat flux and subsurface horizontal and vertical advection (e.g., Jin, 1997; Latif et al., 1998; Xie, 2004), but increasing evidence indicates that extratropical forcings, both from the Southern and Northern Hemisphere, play a nonnegligible role in altering tropical SST variability (e.g., van Loon and Shea, 1985; Vimont et al., 2001, 2003; Chiang and Vimont, 2004; Kang et al., 2008; Terray, 2011; Chen et al., 2014; Zhang et al., 2014a, 2014b; Ding et al., 2015; Hamlington et al., 2015; Yamazaki and Watanabe, 2015; Shi et al., 2016).

Factors in the Southern Hemisphere extratropics that may influence ENSO include the atmospheric circulation, such as the westerly trough (e.g., van Loon and Shea, 1985), a transverse circulation between the tropics and Australia (Hong et al., 2014), extratropical sea level pressure (Hamlington et al., 2015), and extratropical SST (Terray, 2011; Ding et al., 2015; Yamazaki and Watanabe, 2015). Specifically, the strength of the westerly trough over the South Pacific several months before the onset of ENSO plays a role in shaping extreme ENSO events (van Loon and Shea, 1985). A transverse circulation, characterized by a low-level equatorward flow spinning off from a high-pressure anomaly around Australia and an upper-level southward divergent flow branching off from the convection center over the central Pacific, serves as an effective booster during the developing stage of a super El Niño by intensifying tropical Pacific low-level westerly winds (Hong et al., 2014). Southern Hemisphere extratropical sea level pressure variations over the May–July period are excellent predictors of peak ENSO events between November and January (Hamlington et al., 2015). Terray (2011) found that atmospheric variability in the Southern Hemisphere midlatitudes influences ENSO evolution by triggering subtropical SST anomalies in both the Southern Indian and Atlantic oceans. In addition, SST anomalies in the extratropical South Pacific may also have an influence on ENSO (Ding et al., 2015). The corresponding mechanism for Southern Hemisphere extratropical SST to influence ENSO involves the propagation of subtropical SST anomalies into the deep tropics (Terray, 2011; Ding et al., 2015). Recently, Zhang et al. (2014a) pointed out that a robust SST mode exists in the South Pacific, which is named the South Pacific Meridional Mode (SPMM). The SPMM is found to play an important role in triggering ENSO-like variability by regulating the zonal gradients of SST and sea level pressure along the equator (Zhang et al., 2014a). These results are robust in multiple atmospheric general circulation models (AGCMs) coupled with slab ocean models (AGCM–slab models), and are further verified by results from fully coupled models and observations. In addition, Zhang et al. (2014b, 2016) showed that the regulating role of the SPMM on ENSO is dependent on the mean climate state.

Yamazaki and Watanabe (2015) used outputs from the Coupled Model Intercomparison Project, Phase 5, to show that Southern Hemisphere extratropical SST can influence the strength of ENSO. They found that a stronger ENSO, quantified by a larger standard deviation of Niño3 index during a specific period, corresponds to warmer Southern Ocean SSTs during the same period. The mechanism can be generally summarized as: Anomalous Southern Ocean warming can remotely modulate ENSO strength via influencing mean precipitation in the eastern-equatorial Pacific, which is known to affect ENSO strength due to mutual interaction (Watanabe and Wittenberg, 2012). Specifically, warmer Southern Ocean SSTs give rise to an anomalous northward heat transport across the extratropics into the tropics due to a weaker meridional temperature gradient. This induces an anomalous Hadley cell, with an anomalous southward moisture transport in the lower branch (e.g., Chiang and Bitz, 2005; Kang et al., 2008), which further reduces equatorial Pacific precipitation.

Factors that influence ENSO in the Northern Hemisphere extratropics include atmospheric modes such as the North Pacific Oscillation (NPO), North Pacific Meridional Mode (NPMM), and Arctic Oscillation (AO)/Northern Annular Mode (NAM). A possible NPO forcing on ENSO was identified in several pioneering studies (Vimont et al., 2001, 2003; Chiang and Vimont, 2004), and the corresponding mechanism involves the influence of the NPO on subtropical SST and the propagation of subtropical SST anomalies into the deep tropics through wind–evaporation–SST feedbacks. Observational and modeling studies have revealed that the NPMM, which is a counterpart of the SPMM, often acts as a precursor to ENSO events (Chiang and Vimont, 2004; Larson and Kirtman, 2013), and this relationship has been further examined within a forecast framework using a suite of SST hindcasts from the North American multimodel ensemble prediction experiment (Larson and Kirtman, 2014). The AO/NAM can influence winter ENSO through the spring AO/NAM modulation of western tropical Pacific westerlies and its propagation eastwards via Kelvin waves (Chen et al., 2014).

In view of the similarity between the SAM and NAM, it seems reasonable to expect that the SAM may also influence ENSO. In fact, there is increasing evidence to show that the influence of the SAM could impinge on the tropics (e.g., Baldwin, 2001; Thompson and Lorenz, 2004). Specifically, the SAM has been observed to affect tropical meridional circulation and trade winds. For example, Thompson and Wallace (2000) demonstrated that the SAM is characterized by fluctuations in the strength of the trade winds throughout the subtropics in the Southern Hemisphere. Zheng and Li (2012) and Zheng et al. (2015a) pointed out that the December–January–February (DJF) SAM can modulate the March–April–May (MAM) Hadley circulation and trade winds. When the DJF SAM is in a positive phase, counterclockwise and clockwise meridional cells alternately occur

between the Southern Hemisphere midlatitudes and Northern Hemisphere subtropics in MAM. In the tropics, a counterclockwise circulation exists between 10°S and 10°N, alongside anomalous descent and ascent at around 10°N and 10°S, respectively (Zheng and Li, 2012; Zheng et al., 2015a). The present study is motivated by this influence of the DJF SAM on MAM tropical atmospheric circulation (which is known to be closely linked to the evolution of ENSO) and attempts to explore the possible modulation of the DJF SAM on the amplitude of ENSO decay, which usually appears during MAM.

The influences of the above-mentioned extratropical factors on ENSO as revealed by previous studies (e.g., AO/NAM, southern extratropical SST) can be divided into two types. The first type is that extratropical factors play a role in triggering ENSO events through processes such as westerly bursts in the tropical Pacific (e.g., Chen et al., 2014; Ding et al., 2015). The second type is that extratropical factors modulate the amplitude of ENSO by producing additional perturbations on tropical Pacific SST anomalies (e.g., Yamazaki and Watanabe, 2015). This paper focuses on the second type of influence. In short, the aim of this study is to explore the influence of the DJF SAM on the amplitude of ENSO decay.

The remainder of the paper is organized as follows: In section 2, we briefly describe the datasets and methodology used in the study. In section 3, the observed leading correlation between the DJF SAM and amplitude of ENSO decay is presented, and in section 4 the mechanism for this leading correlation is discussed. Finally, a discussion and conclusions are presented in section 5.

2. Data and methodology

2.1. *Reanalysis data*

The atmospheric circulation data used in this study are from the National Centers for Environmental Prediction–National Center for Atmospheric Research (NCEP–NCAR) reanalysis (Kalnay et al., 1996), with a horizontal resolution of 2.5°×2.5°, and the National Oceanic and Atmospheric Administration (NOAA) 20th century reanalysis (20CR), with a resolution of 2.0° × 2.0°. The variables used are horizontal wind, vertical velocity, sea level pressure, geopotential height, and outgoing longwave radiation (OLR). The results from these two datasets are generally consistent, and thus we mainly present the results from NCEP–NCAR in this study. For SST, we use the NOAA Extended Reconstructed SST, version 3b dataset (ERSST.v3b), with a horizontal resolution of 2.5° × 2.5°, and HadISST, developed at the Met Office Hadley Centre, with a resolution of 1.0° × 1.0°. Two global precipitation datasets are used to cross-validate the corresponding results: version 2.2 of the Global Precipitation Climatology Project (GPCP), and the Climate Prediction Center Merged Analysis of Precipitation (CMAP). The horizontal resolution of both these precipitation datasets is 2.5° × 2.5°.

This study concentrates on the DJF and MAM seasons. All meteorological variables are converted to seasonal means before statistical analysis. Unless otherwise stated, the analysis period in this study is from 1950/51 to 2015/16, except for the GPCP and CMAP precipitation datasets, which start from 1979, and for the 20CR OLR dataset, which is now available till 2014. Statistical analyses for the period 1979/80–2015/16 are also conducted in some cases to provide additional evidence for the observed relationship.

2.2. *Model simulation*

Simulations from the "slab ocean control experiment" of 13 AGCM–slab models archived in Phase 3 of the Coupled Model Intercomparison Project (CMIP3) are employed in this study. The details of the CMIP3 models employed are listed in Table 1. Considering that the horizontal resolutions are different among the models, simulations from these AGCM–slab models are interpolated to the same horizontal resolution (2.0° × 2.0°) before calculating the multi-model mean. In the framework of AGCM–slab models, SST variability is determined by the thermodynamic equation, without ocean dynamical processes. Since ocean dynamics play an essential role in controlling ENSO events (Jin, 1997), using results from AGCM–slab models is assumed to provide a convenient way to remove the climatic influence of ENSO and investigate the role extratropical factors in modulating tropical Pacific SST (Zhang et al., 2014a, 2014b, 2016). However, it is important to note that ENSO-type SST variability is shown to exist even without ocean dynamics, under the circumstance of a strong equatorial Pacific cold tongue supporting atmospheric feedback between circulation changes and clouds (Dommenget, 2010). Therefore, before using outputs from a specific set of AGCM–slab models as an approach to exclude ENSO effects, it is important to investigate the strength of ENSO-type variability in the models.

Table 1. List of AGCM–slab models used in this study from the archive of CMIP3. The abbreviations "nLon" and "nLat" mean the number of grids in the zonal and meridional directions, respectively; "nLev" means the number of levels in the vertical direction.

Model names	Simulation length (years)	Resolution	
		nLon × nLat	nLev
CCCma_CGCM3.1_t47	30	96 × 48	17
CCCma_CGCM3.1_t63	30	128 × 64	17
CSIRO Mk3.0	60	192 × 96	17
GFDL CM2.0	50	144 × 90	17
GFDL CM2.1	100	144 × 90	17
GISS-ER	120	72 × 46	17
INM-CM3.0	60	72 × 45	17
MIROC3.2 (hires)	20	320 × 160	17
MIROC3.2 (medres)	60	128 × 64	17
MPI_ECHAM5	100	192 × 96	16
MRI-CGCM2.3.2a	150	128 × 64	17
CCSM3	51	256 × 128	17
HadGEM1	70	192 × 145	16

2.3. *Methodology*

The SAM variability reflects an oscillation in sea level pressure between the middle and high southern latitudes (Fig. 1a). Its variability can be quantified using the SAM index (SAMI; Nan and Li, 2003), which is defined as the difference in normalized zonal-mean sea level pressure between 40°S and 70°S. This SAMI is available at http://ljp.gcess.cn/dct/page/65544. The other measure of SAMI is defined as the leading principal component in the EOF analysis of sea level pressure south of 30°S. Since the standardized time series of these two SAMIs are highly correlated (Fig. 1b), only the results based on the definition reported by Nan and Li (2003) are shown in the following analyses.

Furthermore, to examine the reliability of reanalysis-based SAMI before the satellite era, the station-based SAMI reported by Marshall (2003) is also employed, referred to as SAMI-Marshall. The SAMI-Marshall index can be obtained from https://climatedataguide.ucar.edu/climate-data/marshall-southern-annular-mode-sam-index-station-based. It is based on observational records of sea level pressure from six stations at roughly 65°S and six stations at roughly 40°S, and extends back to 1957. As shown in Fig. 1b, the station-based SAMI-Marshall and the reanalysis-based SAMI are highly consistent, with a correlation coefficient higher than 0.9. Therefore, it is inferred that the reanalysis-based SAMI is relatively reliable. Although the data quality of reanalysis in the Southern Hemisphere extratropics is usually thought to be poor before 1979, the reanalysis data can generally capture the SAMI variability, possibly attributable to the fact that the SAM is a large-scale phenomenon and the calculation of the SAMI only needs large-scale circulation information.

It is clear in Fig. 1b that significant linear trends exist in the SAMI [0.27 (10 yr)$^{-1}$], which is mainly attributable to external forcings such as ozone depletion over Antarctica or increasing concentrations of greenhouse gases (e.g., Gillett and Thompson, 2003; Fogt et al., 2009a; Thompson et al., 2011). Since the linear trend in SAMI is generally beyond the scope of natural variability, detrended SAMI (Fig. 1c) is employed and all other climatic variables used in this study (e.g., SST, atmospheric circulation, precipitation) are detrended prior to statistical analysis.

The Niño3.4 index, defined as the regionally averaged SST over (5°S–5°N, 170°–120°W), is used to represent ENSO variability. The primary statistical methods employed are regression, composite analysis, and correlation analysis. The Student's *t*-test is used to assess the statistical significance of the correlation/regression coefficients and the composite differences. Singular value decomposition (SVD) analysis can determine the coupled modes of orthogonal singular vectors, as well as expansion coefficient correlations from the covariance matrix of two geophysical fields. Here, SVD analysis is used to reveal coupled spatial patterns between DJF sea level pressure over the Southern Hemisphere extratropics and MAM SST over the tropics.

Partial correlation/regression analysis is one of the most commonly used methods to detect the relationship between two variables after removing the effect of the third one. In this study, partial regression is adopted to estimate the connection between two variables after linearly removing the ef-

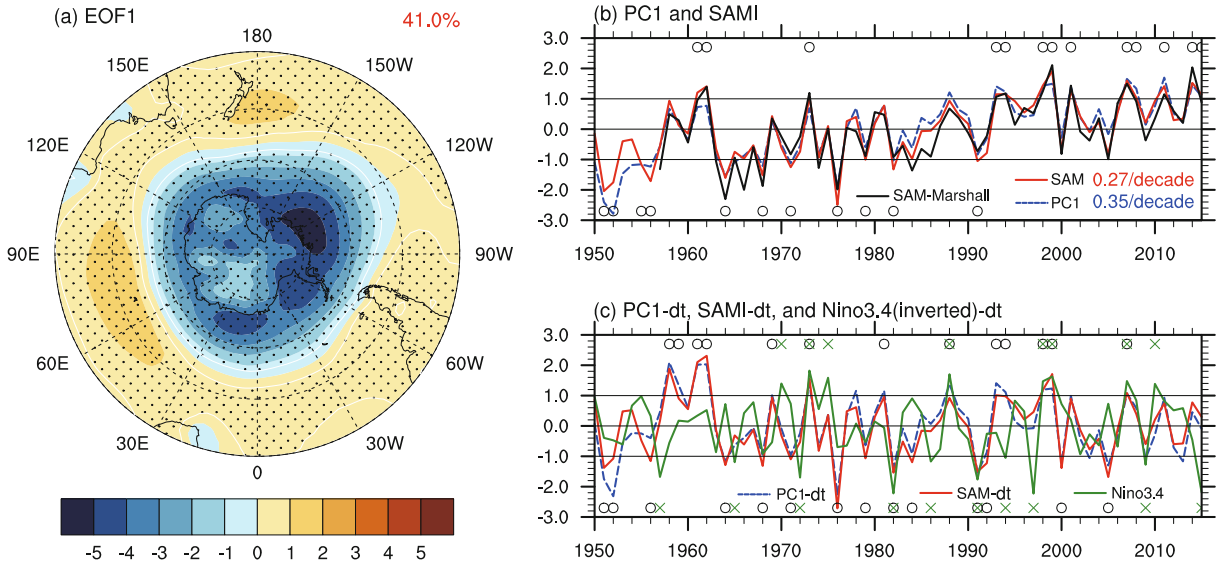

Fig. 1. (a) Spatial pattern of the DJF SAM shown by regressing sea level pressure (units: hPa) on the leading principal component of the EOF analysis of sea level pressure south of 30°S. The red number (top right) indicates the explained variance of the leading mode (41.0%). Stippling represents significance at the 90% confidence level. (b) Normalized time series of the leading principal component (blue), the SAMI (red), and the SAMI-Marshall index (black), in DJF. The corresponding linear trends are noted in the bottom-right corner. The black straight lines indicate the values of −1 and 1, and circles mark positive (negative) SAM years with a threshold of ±1.0 standard deviation. (c) As in (a), but for the detrended time series. The green line in (c) denotes the inverted DJF Niño3.4 index, and the green crosses mark El Niño and La Niña years with a threshold of ±1.0 standard deviation.

fect of DJF ENSO. Note that completely removing variations related to a specific variable from the observations is always challenging, due to ambiguities arising from nonlinear influences (e.g., Compo and Sardeshmukh, 2010; Zhang et al., 2014a, 2014b, 2016), and partial regression may not completely exclude the signal of the third variable in the presence of nonlinear effects.

2.4. *Momentum balance*

The momentum balance is used to understand the variability of mean meridional circulation (MMC). Walker and Schneider (2006) introduced a local Rossby number (herein R_o) that measures the importance of eddies driving the MMC. It is expressed as

$$R_o = -\frac{\bar{\zeta}}{f}\,, \tag{1}$$

where the overbar represents a zonal mean, ζ is the relative vorticity, and f is the Coriolis parameter. The smaller (larger) the value of R_o is, the larger (smaller) the role of eddy stress. The red contours in Fig. 2a show the climatological mean R_o in MAM. It is below 0.5 in most regions of the tropics, indicating that the MAM MMC in this region is in an intermediate regime between the eddy-driven and axisymmetric (involving angular momentum conservation) limits. In contrast, the climatological-mean R_o in the extratropics is very small, indicating the MMC is almost eddy-driven (Kang et al., 2011; Kang and Lu, 2012).

The zonal-mean zonal wind equation is written as

$$\frac{\partial \bar{u}}{\partial t} \approx \bar{v}(f+\bar{\zeta}) - S\,, \tag{2}$$

where $f+\bar{\zeta}$ is the absolute vorticity of the zonal-mean flow, $\bar{v}$ is the meridional wind, and S is the horizontal eddy momentum flux divergence ($S = 1/(\cos^2\phi)\partial/(\partial\phi)\overline{u'v'}\cos^2\phi$), in which ϕ represents latitude and a prime means zonal deviation. The first term on the right-hand side of Eq. (2) reflects the meridional transport of vorticity by the zonal-mean flow. The second term reflects the eddy stress. The climatology of MAM S is shown in Fig. 2a (shading), from which it can be seen that divergence occurs in the upper troposphere in the low and high latitudes, and convergence occurs in the midlatitudes.

Setting the tendency term in Eq. (2) equal to zero and using the definition of R_o as expressed in Eq. (1), the momentum balance is obtained:

$$(1-R_o)f\bar{v} \approx S\,. \tag{3}$$

To verify the applicability of the momentum balance shown in Eq. (3), the long-term average values of different terms in Eq. (3) are presented in Fig. 2b. Although biases exist, the upper-level momentum balance is captured relatively well by Eq. (3) at most latitudes. The eddy stress S in Eq. (3) can be divided into the contributions from transient eddies and stationary eddies, referred to as $S_{\rm tr}$ and $S_{\rm st}$, respectively. Figure 2b also shows the allocation of the eddy stress to stationary $S_{\rm st}$ and transient $S_{\rm tr}$ components. The contributions from stationary and transient eddies are of comparable magnitude in the Northern Hemisphere, whereas the transient eddy stress is larger in the Southern Hemisphere (Fig. 2b).

In the tropics, it is reasonable to linearize the momentum budget because the interannual variability of the tropical MMC is small compared with the climatological mean (Ca-

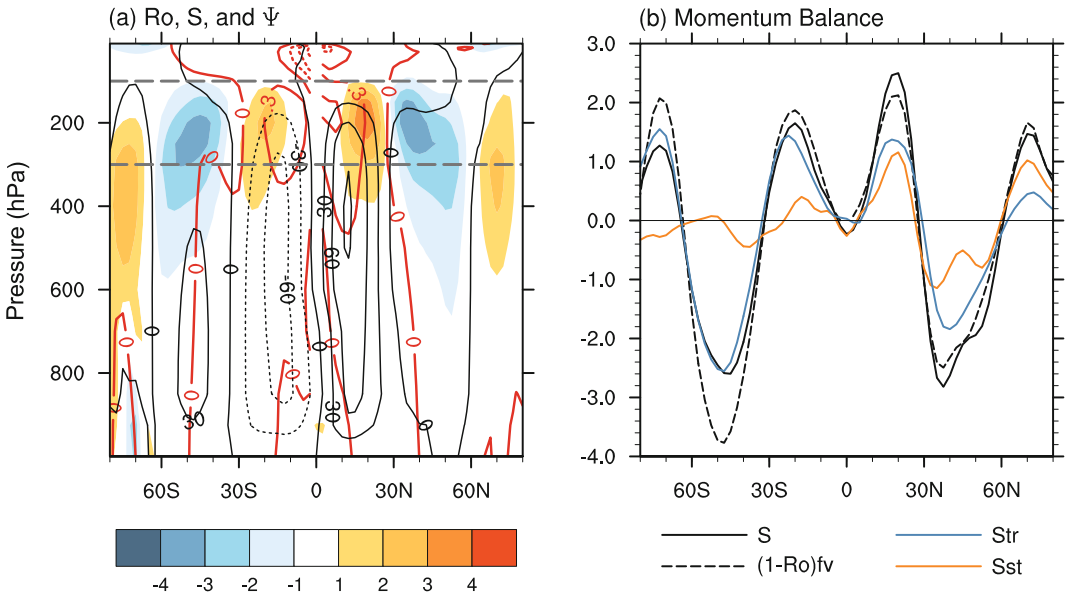

Fig. 2. (a) Zonal-mean mass streamfunction (Ψ, black contours; units: 10^9 kg s^{-1}), eddy momentum flux divergence (S; color shading; units: 10^{-5} m s^{-2}), and the Rossby number R_o (red contours; interval: 0.3), in MAM. The two gray dashed lines mark the 300 and 100 hPa levels. (b) Momentum budget in Eq. (3), averaged between 300 and 100 hPa: $(1-R_o)f\bar{v}$ (black dashed line); S (black solid line); and contributions of stationary (orange) and transient (blue) components of S. The units for the above terms in (b) are 10^{-5} m s^{-2}.

ballero, 2007). By doing this, it is possible to distinguish the relative roles of R_o and S in the changes in the MMC. As introduced in Caballero (2007), the linearized momentum budget in the tropics can be expressed as

$$\delta\bar{v} \approx \frac{\bar{v}}{1-R_o}\delta R_o + \frac{1}{(1-R_o)f}\delta S \ , \tag{4}$$

where δ indicates an interannual fluctuation around the climatological mean. Thus, the increased mass flux of the MMC can be balanced by an increased δR_o term, or by an increased eddy stress δS term.

In the extratropics, where R_o is smaller than in the tropics (Fig. 2a), the MMC can be considered as determined solely by the eddy stress:

$$\delta\bar{v} \approx \frac{1}{f}\delta S \ . \tag{5}$$

Therefore, the increased mass flux of the MMC is mainly balanced by increased eddy stress S.

Momentum balance is most applicable above the lower-troposphere layer because of weak friction dissipation. According to the law of mass conservation, changes in upper-tropospheric circulation will result in changes in lower-tropospheric circulation. For example, convergence in the upper troposphere tends to lead to descending motion and divergence in the lower troposphere, and thus the occurrence of an anomalous meridional circulation.

3. Link between the DJF SAM and amplitude of ENSO decay

To facilitate the investigation of interannual variability, some of the basic aspects of the climatology in MAM are shown in Fig. 3. Figure 3a shows that the warmest SST in MAM is located in the western Pacific. Accordingly, the main center of horizontal wind divergence in the upper troposphere

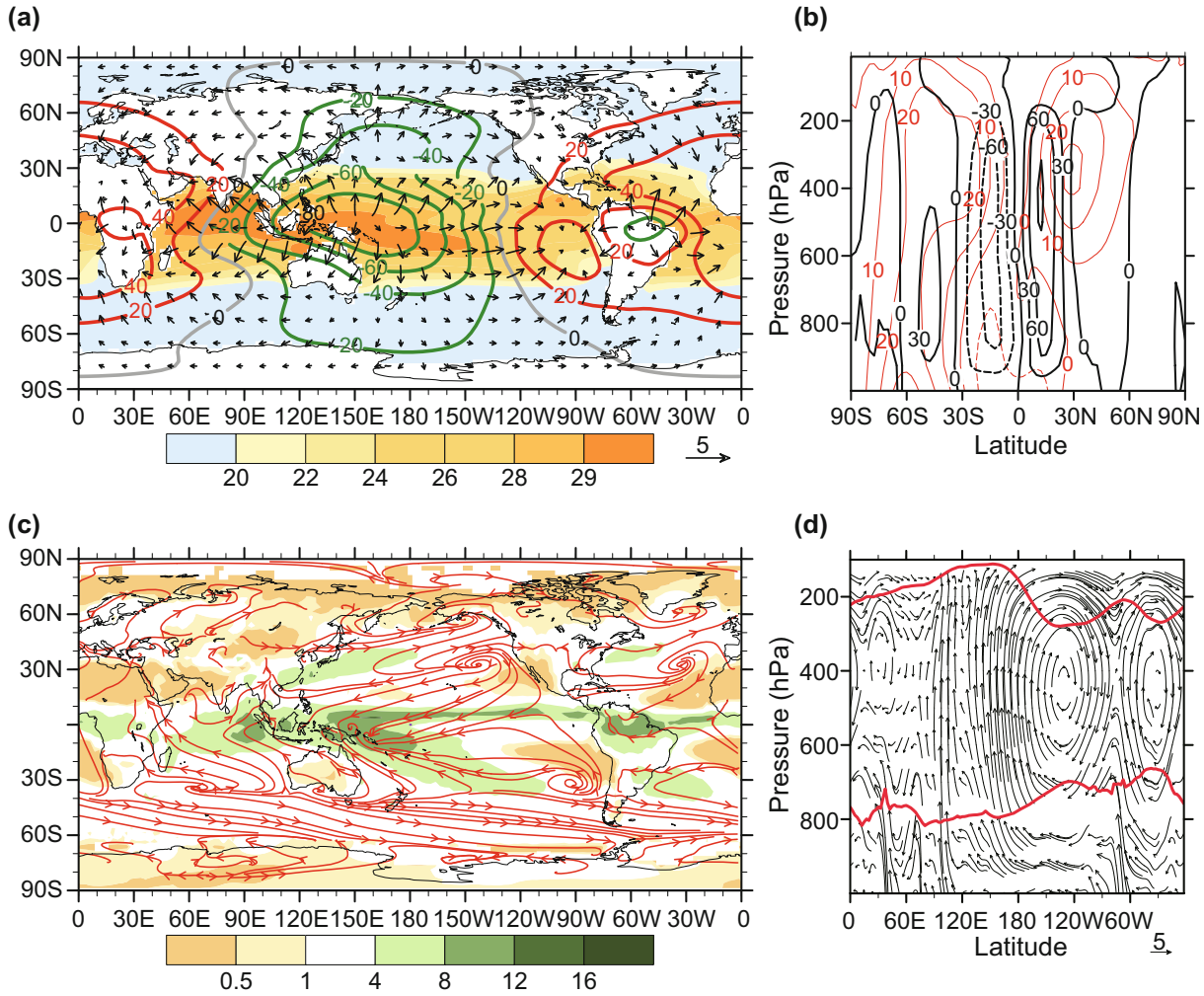

Fig. 3. Climatological mean field of MAM (a) SST derived from HadISST (shading; units: °C), divergent wind at 200 hPa (arrows; units: m s^{-1}), and velocity potential (contours; units: 10^6 m^2 s^{-1}), with green/red lines for positive/negative values; and (b) zonal-mean mass streamfunction (black contours; units: 10^9 kg s^{-1}) and zonal wind (red contours; units: m s^{-1}). (c) CMAP precipitation (shading; units: mm d^{-1}) and surface wind (streamlines; units: m s^{-1}); and (d) meridional zonal circulation (arrows; units: m s^{-1}) averaged between 30°S and 30°N. In (d), the vertical velocity was amplified by 10^4 times, and the red lines qualitatively indicate the zonal deviation of surface pressure and geopotential height at 200 hPa.

(200 hPa) is located in the western Pacific (Fig. 3a). The distribution of velocity potential in the lower troposphere (not shown) is opposite to that in the upper troposphere, where the divergence center over the western Pacific is replaced by a convergence center. As shown in Fig. 3b, The Hadley Cell has a clear equatorial symmetry that is roughly bounded by 30°S and 30°N, with ascending air close to the equatorial belt and descending air between 15°N (S) and 30°N (S), in both hemispheres. Tropical meridional winds diverge in the upper troposphere and converge in the lower troposphere. The lower-tropospheric convergence corresponds to the position of the Intertropical Convergence Zone (ITCZ), and is accompanied by strong precipitation along the equator (Fig. 3c). As shown in Fig. 3d, the geopotential height in the lower (upper) troposphere over the western Pacific is lower (higher) than that over the eastern Pacific. Strong ascending air occurs over the warm pool and descending air occurs over the eastern tropical Pacific (Fig. 3d), which is a manifestation of the Walker circulation.

3.1. *Correlation between the DJF SAM and MAM tropical Pacific SST*

Figure 4a shows the correlation between the DJF SAM and MAM SST for the period 1950/51–2015/16 derived from HadISST. A significant negative correlation exists in the central tropical Pacific (Niño3.4 region). This negative correlation also exists for the period 1978/79–2015/16 (Fig. 4b). In addition, Figs. 4c and d show the correlation coefficients derived from ERSST.v3b. The negative correlation over the Niño3.4 region from ERSST.v3b is in good agreement with that from HadISST. The following analyses mainly show results from HadISST, which is characterized by a higher horizontal resolution. Besides, Fig. 4 shows that the DJF SAM is positively correlated with MAM SST over the western North Pacific, which has also been found to be associated with ENSO (Wang et al., 2000; Feng and Li, 2011; Wang et al., 2012a, 2012b) but is not the focus of the present study.

Figure 5 shows the results from the SVD analysis applied to the DJF sea level pressure south of 20°S and MAM SST fields between 30°S and 30°N to reveal their coupled spatial pattern. The first coupled mode between the DJF extratropical sea level pressure and MAM tropical SST is responsible for 60% of the squared covariance fraction. As shown in Fig. 5a, the associated time series of DJF sea level pressure and MAM SST exhibit strong covariability, yielding a correlation coefficient of 0.74 (significant at the 99% confidence level). Figure 5a also shows the time series of the DJF SAMI, from which it is apparent that the DJF SAM is in strong agreement with the expansion coefficient of the first coupled mode of DJF sea level pressure, with a correlation coefficient of 0.74 (significant at the 99% confidence level). The distribution of DJF sea level pressure in the first coupled mode from

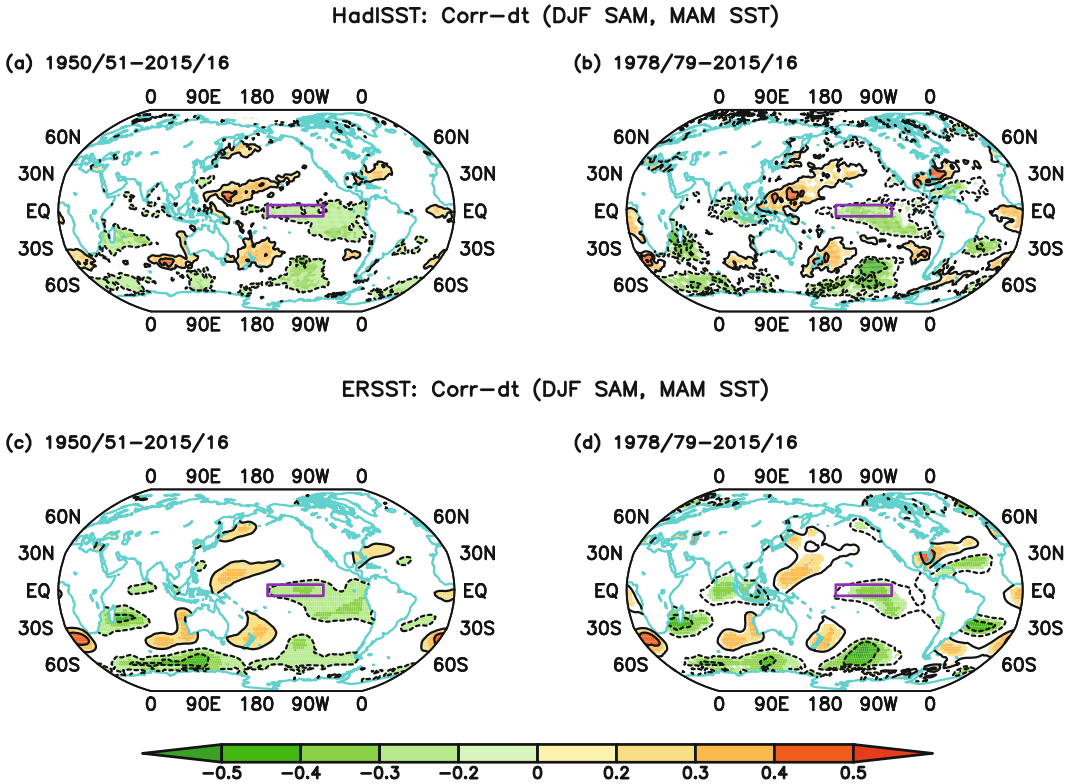

Fig. 4. Correlation coefficients between the DJF SAM and MAM SST for the periods (a, c) 1950/51–2015/16 and (b, d) 1978/79–2015/16, derived from (a, b) HadISST and (c, d) ERSST.v3b. Values not significant at the 90% confidence level are masked out as white shading. Solid (dashed) contours represent positive (negative) values with an interval of 0.2. The Niño3.4 region is indicated by the purple box.

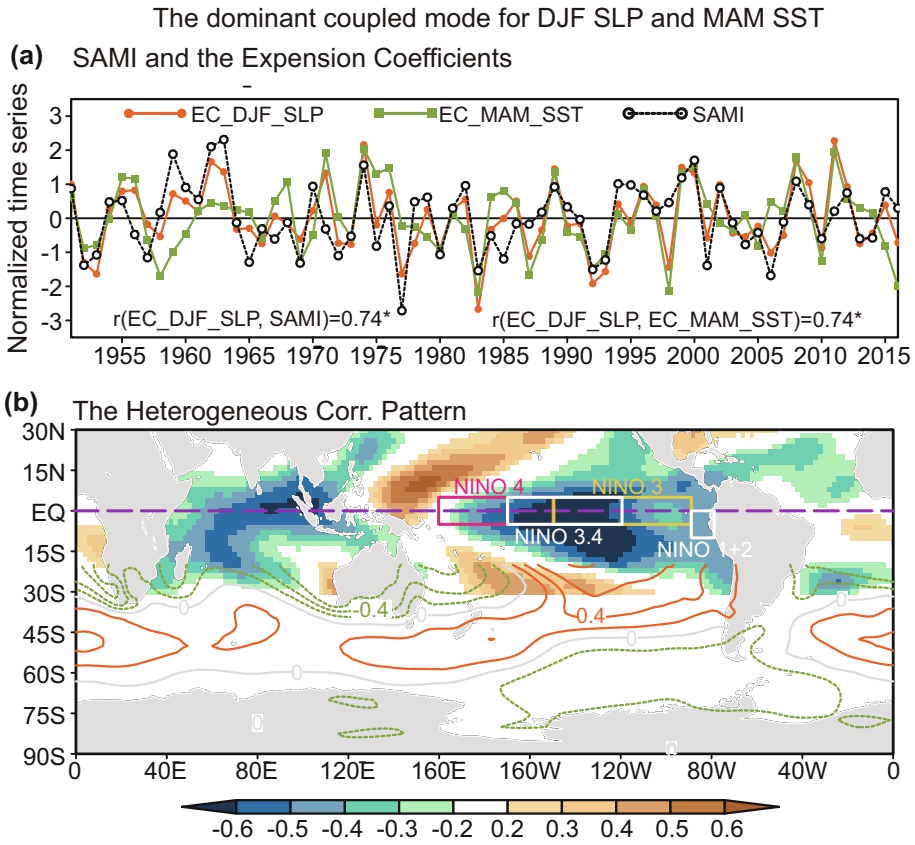

Fig. 5. (a) The normalized expansion coefficients of the DJF sea level pressure (solid orange line) and MAM SST (solid green line) for the first dominant coupled mode of the SVD. Also shown are the normalized time series of SAMI (dotted black line). (b) The heterogeneous correlation pattern for the first dominant coupled mode of DJF sea level pressure south of 20°S (contours with interval of 0.2) and MAM tropical SST between 30°S and 30°N (shading) in the SVD analysis. The purple line indicates the position of the equator.

the SVD analysis corresponds to the typical positive SAM polarity, which is characterized by positive sea level pressure anomalies over the midlatitudes and negative anomalies over high latitudes (Fig. 5b). The first coupled mode of the MAM SST appears as a negative correlation in the central and eastern tropical Pacific, with the strongest correlation in the Niño3.4 region (Fig. 5b). Therefore, it is expected that when the DJF SAM is in a positive (negative) phase, there tends to be cooler (warmer) SST in the Niño3.4 region, which is consistent with the results from the correlation analysis shown in Fig. 4.

3.2. *Link between the DJF SAM and MAM ENSO*

The above results reveal a negative correlation between the DJF SAM and MAM tropical Pacific SST, and the spatial distributions of the negative correlation in the tropical Pacific cover most of the regions used to define typical ENSO indices (Niño3.4, 3, 4, and 1+2). Given that the strongest negative correlation between the DJF SAM and MAM tropical Pacific SST exists in the Niño3.4 region (Figs. 4 and 5), the Niño3.4 index is used to represent the ENSO variability in the following analysis.

Figures 6a and b show the composite DJF SST anomalies for El Niño and La Niña years with an absolute value of the DJF Niño3.4 index greater than a standard deviation of 0.5, respectively. Warmer and colder SST anomalies are clearly evident over the Niño3.4 region, respectively. The autocorrelation between the DJF and MAM Niño3.4 index is 0.76, illustrating the strong persistence of the DJF ENSO signal. Figures 6c and d show the composite MAM SST anomalies for positive and negative DJF Niño3.4 index with a threshold of ±0.5 standard deviation, respectively. It is found that El Niño-like and La Niña-like SST anomalies are still significant during MAM, which is mainly attributable to the persistence of the DJF ENSO signal. When there is an El Niño (La Niña) condition in DJF, there tends to be warmer (cooler) SST anomalies over the tropical Pacific during the following MAM, with the strength weaker than those during DJF, which is a manifestation of ENSO decay.

Figures 6e and g are similar to Fig. 6c except the composite analysis consists of positive Niño3.4 index, with positive and negative DJF SAMI with a threshold of ±0.5 standard deviation, respectively. Comparing Figs. 6e and g illustrates that the El Niño–like SST anomalies over the central Pacific

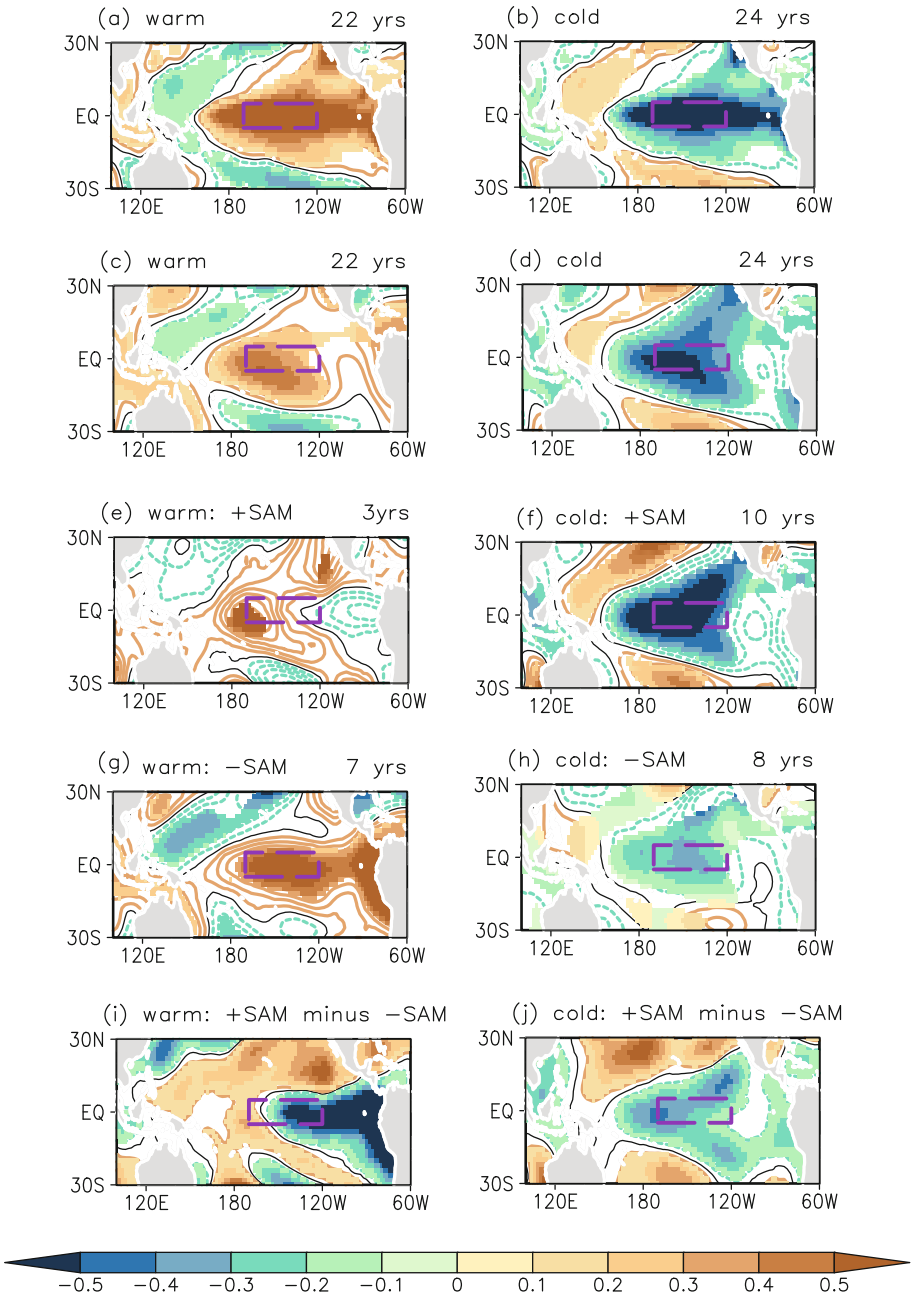

Fig. 6. Composite DJF SST anomalies for (a) positive and (b) negative DJF Niño3.4 years with a threshold of ±0.5 standard deviation. The contour interval is 0.1°C, and values not significant at the 90% confidence level are masked out as white shading. The Niño3.4 region is indicated by the purple dashed box. The sample size of the composite analysis is labeled in the top-right corner of the panel. (c, d) As in (a, b) but for MAM SST anomalies. (e) Composite MAM SST anomalies for positive DJF Niño3.4 with positive DJF SAM years and with a threshold of ±0.5 standard deviation. (f–h) As in (e) using the threshold of ±0.5 standard deviation, but for (f) negative Niño3.4 with positive SAM, (g) positive Niño3.4 with negative SAM, and (h) negative Niño3.4 with negative SAM, respectively. (i) The difference between (e) and (g). (j) The difference between (f) and (h).

during MAM corresponding to the positive DJF SAM are cooler than those corresponding to the negative DJF SAM. The differences between the positive and negative DJF SAM are shown in Fig. 6i, in which cooling exists in the central and eastern tropical Pacific with maximum anomalies in the eastern tropical Pacific. Similarly, the La Niña-like SST pattern in MAM corresponding to the positive DJF SAM (Fig. 6f) is cooler in the central tropical Pacific than the corresponding negative DJF SAM (Fig. 6h). The differences between the positive and negative DJF SAM show a cooling in the central

tropical Pacific (Fig. 6j), despite the cooling being relatively weaker and extending farther west than that in Fig. 6i. Although differences exist between the warm and cold phases (Figs. 6i and j), the Niño3.4 region being characterized by cooler SST anomalies is a common feature in both phases.

But how can the correlation between the DJF SAM and MAM ENSO be understood? As mentioned in the introduction of this paper, the influences of extratropical factors on ENSO reported in previous studies can be divided into two types, including triggering ENSO events or modulating the amplitude of ENSO. Figure 6 suggests that the DJF SAM may influence the amplitude of ENSO decay during MAM by producing additional SST anomalies over the Niño3.4 region. Although the variances of MAM ENSO/tropical Pacific SST explained by the DJF SAM are smaller than those by the DJF ENSO, influences of the DJF SAM on MAM tropical Pacific SST may overlay on the influence of the DJF ENSO. Hence, the negative correlation between the DJF SAM and MAM tropical Pacific SST reflects the possible influence of the DJF SAM on the amplitude of ENSO decay.

3.3. *Removing the DJF ENSO effects*

As the tropical SST is closely linked to local precipitation and convection, the connection between climate in the central tropical Pacific and the DJF SAM is further explored using tropical OLR and precipitation, which reflects the strength of tropical convection. There are 13 (14) years in which SAMI values are more (less) than one standard deviation above (below) the mean during the period 1950/51–2015/16 (Fig. 1c), referred to as high and low SAM years, respectively. The composite differences in the MAM OLR from 20CR between the positive and negative DJF SAM years are shown in Fig. 7a. Positive anomalies exist over the Niño3.4 region and the adjacent area to the west of the Niño3.4 region, indicating

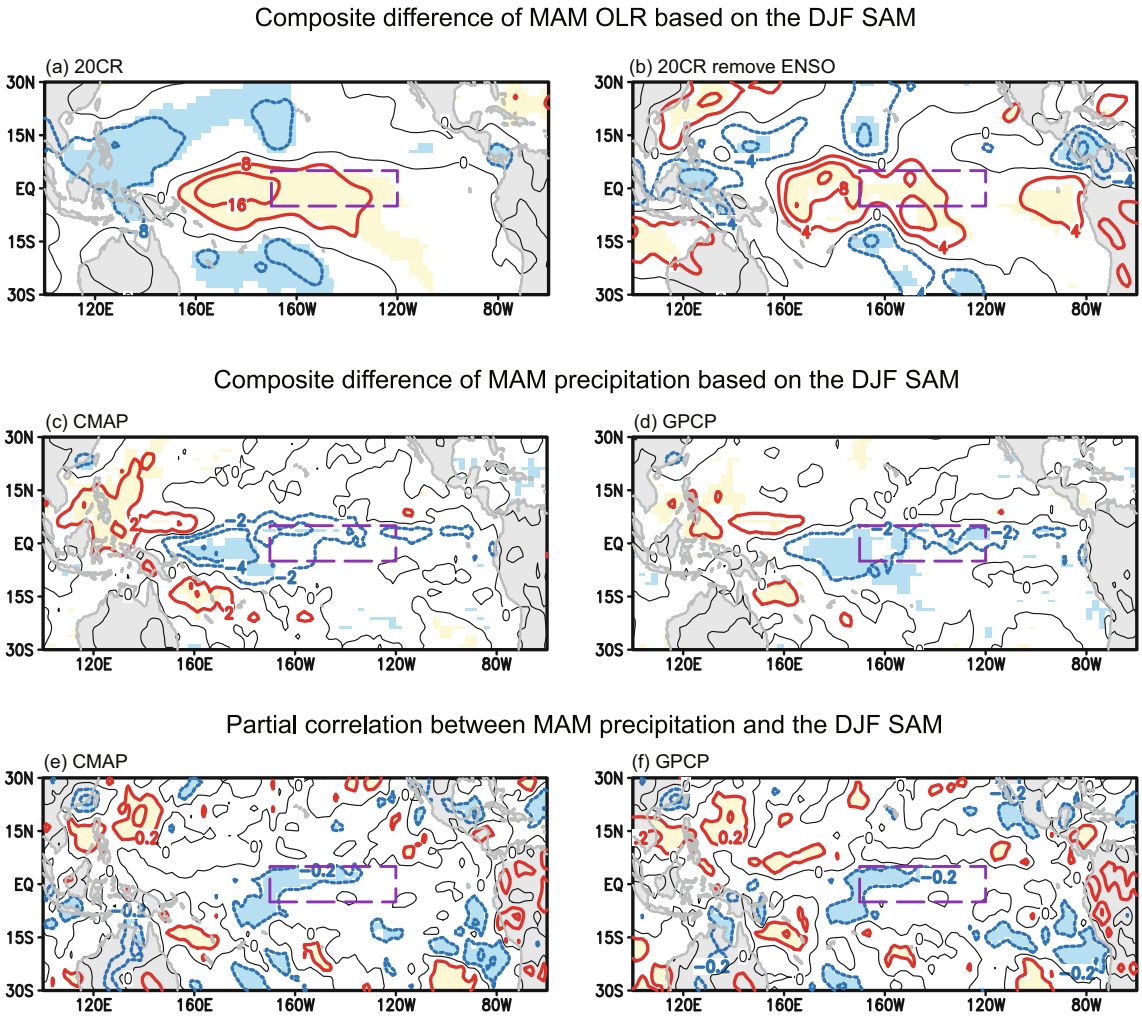

Fig. 7. (a) Composite difference in MAM OLR from 20CR between high and low DJF SAM years (contour interval: 8 W m^{-2}). The definitions of high and low SAM years are described in section 3.3. The shading shows significance at the 90% confidence level. The Niño3.4 region is indicated by the purple dashed box. (b) As in (a), except the typical ENSO years have been excluded when conducting the composite analysis, and the contour interval is 4 W m^{-2}. (c, d) As in (a) but for MAM (c) CMAP and (d) GPCP precipitation (contour interval: 2 mm d^{-1}). (e, f) Partial correlation (contour interval: 0.2) between the DJF SAM and MAM (e) CMAP and (f) GPCP precipitation after removing the DJF ENSO signals.

that convection in these regions is reduced (enhanced) when the DJF SAM is in a positive (negative) phase, which is consistent with a cooler (warmer) SST over the Niño3.4 region. The westward shift of the center of convection anomalies (Fig. 7a) compared with the center of SST anomalies (Fig. 4a) agrees with the typical spatial configuration between SST anomalies and convection anomalies in the tropical Pacific, in which the convection anomalies center tends to exist to the west of the SST anomalies center.

It can be seen in Fig. 1c that the SAM years used to conduct the composite analysis in Fig. 7a include typical El Niño/La Niña years, which are defined by the Niño3.4 index exceeding one standard deviation, and are marked by green crosses in Fig. 1c. Previous studies have revealed that the DJF ENSO plays a significant role in shaping the contemporaneous DJF SAM (e.g., Zhou and Yu, 2004; Fogt and Bromwich, 2006; L'Heureux and Thompson, 2006; Gong et al., 2010; Ding et al., 2012; Ciasto et al., 2015). As a result, the influence of the DJF SAM on MAM ENSO needs to be further verified by removing the DJF ENSO effects. To exclude the influence of DJF ENSO, similar composite analyses as in Fig. 7a are carried out after filtering out the typical ENSO years, and the results are shown in Fig. 7b. What we find is that, in the absence of ENSO events, the MAM OLR anomalies related to the DJF SAM are still obvious.

The composite differences in MAM precipitation from CMAP and GPCP between the positive and negative DJF SAM years are shown in Figs. 7c and d, respectively. These two datasets generate similar results; i.e., tropical precipitation shows some decreases (increases) over the Niño3.4 region and its adjacent area when the DJF SAM is in a positive (negative) phase, which is in accordance with the decreases (increases) in tropical convection over this region (Figs. 7a and b). To exclude the influence of DJF ENSO, partial correlation coefficients between the DJF SAM and MAM precipitation from CMAP and GPCP are shown in Figs. 7e and f. The results show consistency with those in Figs. 7c and d, illustrating the link between tropical Pacific precipitation in MAM and the DJF SAM still exists in the absence of ENSO effects. The reason for using partial correlation is that the two precipitation datasets start from 1979. If employing composite analysis after excluding the typical ENSO years as in Fig. 7b, there are only five low SAM years and three high SAM years, and the sample size is not large enough to obtain robust conclusions. Since the atmospheric circulation, precipitation and SST in the tropics are closely connected, the links between MAM tropical OLR/precipitation and the DJF SAM provide additional evidence for the influence of the DJF SAM on the MAM tropical Pacific SST.

A variety of methods have been proposed for removing ENSO-related components from climate records. Aside from partial correlation/regression, one convenient approach is thought to be the AGCM–slab ocean model framework (Zhang et al., 2014a, 2014b). The AGCM–slab framework excludes dynamical couplings between the ocean and atmosphere, which is the key process giving rise to ENSO. Nonetheless, in view of the existence of ENSO-type variability without ocean dynamics and its model independence (Dommenget, 2010), it is important to explore the strength of ENSO-type variability in AGCM–slab model simulations. Figure 8a shows the multi-model mean of standard deviations of SST from all the 13 AGCM–slab models employed in this study. There is no strong SST variability in the equatorial Pacific in the AGCM–slab simulations (Fig. 8a) in comparison with the observation (Fig. 8b). The modeled regional-averaged standard deviation of SST over the Niño3.4 area is 0.28°C, which in the observation is 0.97°C. Consequently, it is reasonable to believe that ENSO-type variability in the AGCM–slab simulations employed in this study is relatively weaker than the observation.

The relatively weaker ENSO variability in the AGCM–slab models employed in this study helps ensure the removal of the influence of the DJF ENSO on DJF SAM. The multi-model mean of regressed DJF sea level pressure and surface wind on the DJF SAMI is shown in Fig. 9a. One of the dominant features in Fig. 9a is lower (higher) geopotential height in high (mid) latitudes, accompanied by strengthened (weakened) westerlies at around 60°S (40°S), which reflects a typical SAM signal. This implies that the multi-model mean of these AGCM–slab models can capture the SAM activity. In addition, there is no obvious sea level pressure and surface wind anomalies in the tropical Pacific, suggesting that SAM variability in these AGCM–slab models is not influenced by tropical Pacific variability.

To investigate link between the DJF SAM and MAM tropical Pacific SST simulated by the AGCM–slab models, the multi-model mean of regressed MAM SST on DJF SAMI is shown in Fig. 9b. There are cooler SST anomalies in the Niño3.4 region during MAM, implying a negative correlation between MAM central tropical Pacific SST and the DJF SAM, which agrees with observations (Figs. 4–6). Although responses of tropical SST during MAM to the preceding DJF SAM in the AGCM–slab simulations tend to be weaker than observed, which is due to less of an amplification mechanism for tropical SST (e.g., feedback processes related to air–sea dynamical coupling) in the AGCM–slab models, SST anomalies over the Niño3.4 region provide evidence for the connection between MAM tropical Pacific SST and the preceding DJF SAM. Since the DJF SAM is not affected by DJF ENSO in the AGCM–slab models (Fig. 9a), the model-simulated negative correlation between DJF SAM and MAM central tropical Pacific SST is independent of DJF ENSO effects. Furthermore, regressed DJF sea level pressure on regionally averaged SST over the Niño3.4 area in MAM is also shown in Fig. 9b. In the southern extratropics, the regression pattern is characterized by higher pressure in high latitudes but lower pressure in middle latitudes, which represents a negative SAM phase. The pattern correlation between sea level pressure anomalies in Figs. 9a and b is −0.94. This result suggests that when warmer SST anomalies occur in the Niño3.4 region during MAM, there tends to be a negative SAM in the preceding winter, thus further verifying the negative correlation between the DJF SAM and MAM central tropical Pacific SST.

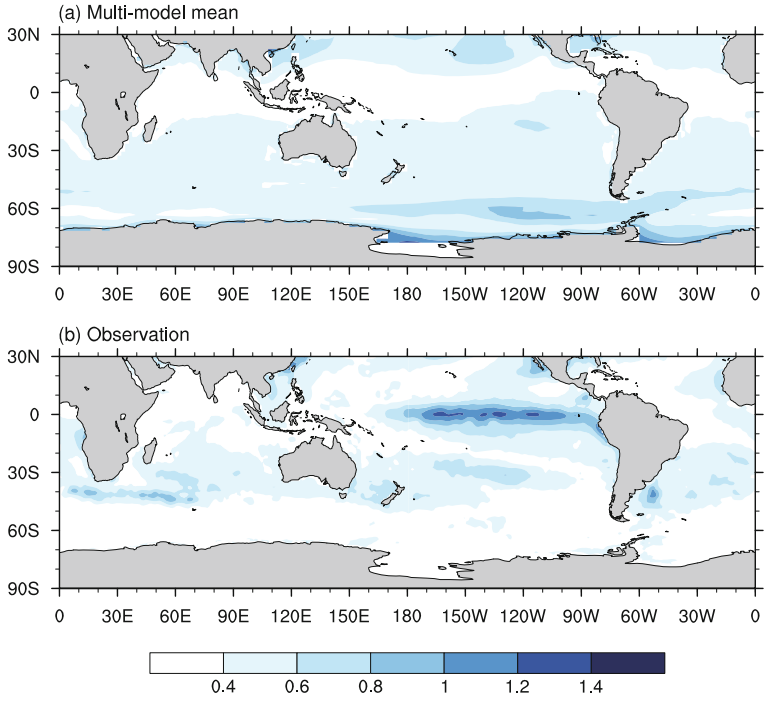

Fig. 8. Standard deviations of DJF SST derived from (a) the multi-model mean of 13 AGCM–slab models, as listed in Table 1, and from (b) observations.

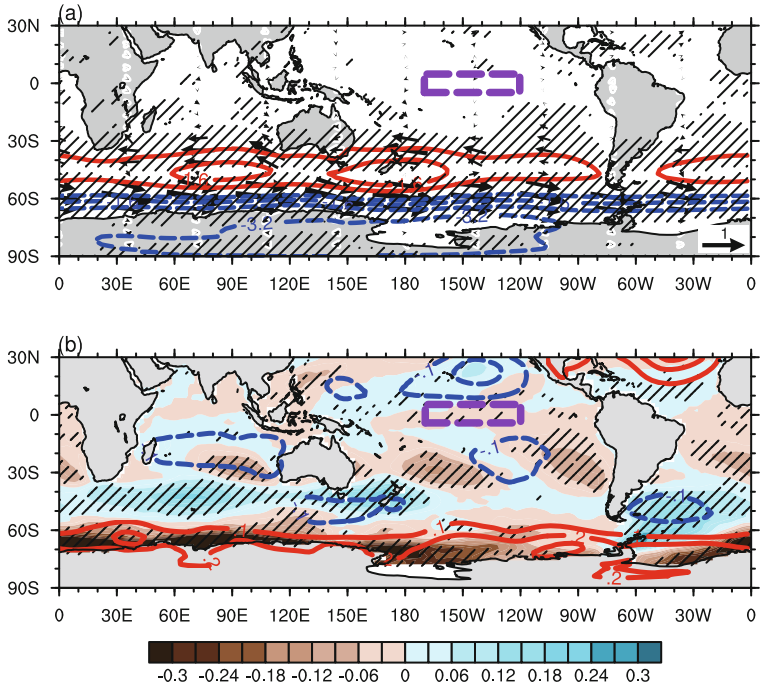

Fig. 9. Multi-model mean of 13 AGCM–slab models. (a) Regression of DJF sea level pressure (contours; interval: 0.8 hPa) and surface wind (vectors units: m s^{-1}) on the DJF SAMI. Solid red (dashed blue) contours represent positive (negative) values. The vectors are displayed every 18 grids in the zonal direction, and every 3 grids in the meridional direction. (b) Regression of MAM SST (shading; units: °C) on the DJF SAMI, and regression of DJF sea level pressure (contours; interval: 0.1 hPa) on regionally averaged SST over the Niño3.4 area in MAM. Solid red (dashed blue) contours represent positive (negative) values. Hatched areas mean the multi-model mean is significant, which is defined as when at least 10 out of 13 models have the same sign as the multi-model mean. The Niño3.4 region is indicated by the purple dashed box.

Similar analysis as in Fig. 6 but derived from the AGCM–slab simulations is shown in Fig. 10. The results show that El Niño-like SST anomalies over the Niño3.4 region during MAM corresponding to positive DJF SAM are cooler than those corresponding to negative DJF SAM, and that the La Niña-like SST anomalies over the Niño3.4 region during MAM corresponding to positive DJF SAM are cooler than those corresponding to negative DJF SAM. Although

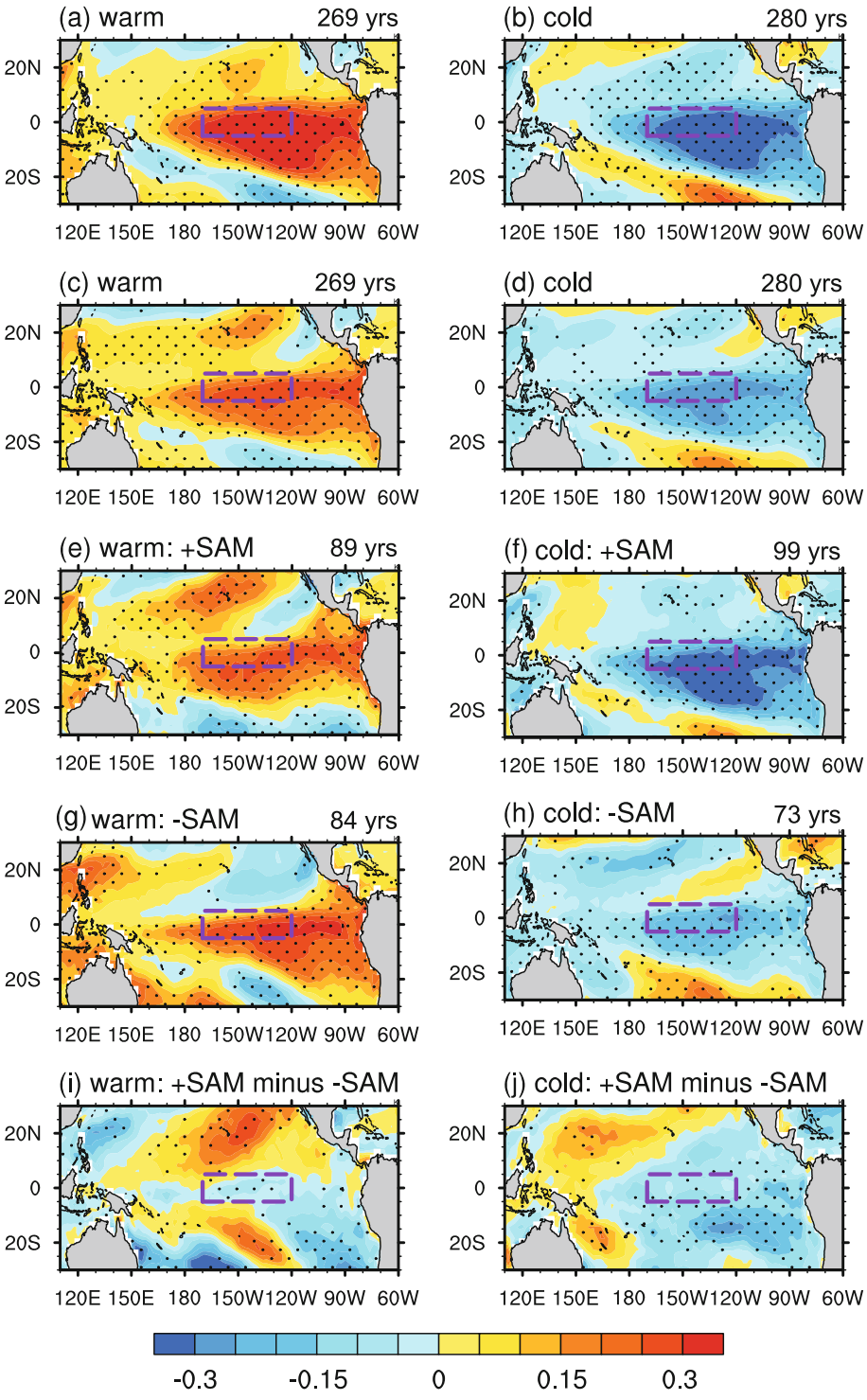

Fig. 10. As in Fig. 6, but for the multi-model mean of 13 AGCM–slab models. The sample size of the composite analysis from all 13 models is labeled on the top-right corner of the panel. Stippling indicates the multi-model mean is significant, which is defined as when at least 10 out of 13 models have the same sign as the multi-model mean. The Niño3.4 region is indicated by the purple dashed box.

the strength of tropical SST anomalies in the AGCM–slab simulations (Fig. 10) tend to be weaker than observed (Fig. 6), a basic agreement between the observation and simulation exists over the Niño3.4 region, verifying the role of the DJF SAM in influencing the amplitude of ENSO decay.

4. Mechanisms

4.1. *Role of the Southern Ocean Dipole*

What mechanisms drive the cross-seasonal influence of the DJF SAM on MAM central tropical Pacific SST? Previous studies have suggested that the persistence of Southern Hemisphere extratropical SST anomalies caused by the SAM plays an important role in transmitting the SAM signals to the following season (Watterson, 2000; Deser et al., 2003, 2010; Gupta and England, 2006; Wu et al., 2009; Thompson et al., 2011; Zheng and Li, 2012; Li et al., 2013; Li, 2016; Zheng et al., 2015a, 2015b). Therefore, it is expected that SST anomalies over the Southern Hemisphere extratropics caused by the DJF SAM may play a role in the cross-seasonal influence of the DJF SAM on the amplitude of MAM ENSO.

Figure 11a shows the partial regression of DJF SST on the DJF SAM after excluding the DJF ENSO signal derived from reanalysis datasets. The DJF SAM is correlated with a dipole-like SST anomaly pattern in the Southern Hemisphere extratropics, with generally warmer (cooler) and cooler (warmer) SST anomalies in the middle and high latitudes when the SAM is in a positive (negative) phase. This SAM-related SST anomaly pattern is referred to as the Southern Ocean Dipole (SOD), and an SOD index is defined as the difference in zonal-mean SST anomalies between 40°S and 60°S (Liu et al., 2015; Zheng et al., 2015a, 2015b). The correlation between the DJF SAM and DJF SOD is 0.61, suggesting an influence of the DJF SAM on the contemporaneous DJF SOD.

The mechanism for the formation of the SAM–SOD relationship has been well documented in previous studies, and can be summarized as follows: Surface wind anomalies caused by the SAM alter local SST through both dynamic and thermodynamic processes, such as Ekman currents and the perturbation of ocean temperature below the surface. Specifically, when the SAM is in a positive phase, strengthened westerlies occur in high latitudes, and thus SST is cooler because of increased loss of heat by turbulent heat flux and cooler Ekman heat transport. In contrast, westerlies in mid-latitudes are weakened when the SAM is in a positive phase, and thus SST is warmer because of a decreased loss of heat and warmer Ekman heat transport (Watterson, 2000; Cai and Watterson, 2002; Lefebvre et al., 2004; Gupta and England, 2006; Wu et al., 2009; Thompson et al., 2011; Zheng and Li, 2012).

Owing to the large heat capacity of the ocean, the DJF SOD caused by the DJF SAM extends to the following MAM (Wu et al., 2009; Zheng and Li, 2012; Li et al., 2013; Zheng et al., 2015a, 2015b; Li, 2016; Fig. 11b). The correlation between the DJF and MAM SOD indices is 0.81 and the pattern correlation between Figs. 11a and b is 0.91, implying a strong persistence of the DJF SOD signal. In view of the strong persistence of the SOD, the DJF SAM is significantly correlated with the MAM SOD, with a correlation coefficient of 0.55. The persistence of the DJF SAM–induced SOD provides a mechanism for the transmission of the DJF SAM signal to the following MAM.

The correlation between the MAM SOD and MAM ENSO is −0.42, implying a potential role of the MAM SOD in influencing tropical Pacific SST during MAM. To remove the influence of DJF ENSO, partial regressions of Southern Hemisphere extratropical SST during DJF and MAM on MAM Niño3.4 index are shown in Figs. 11c and d, respectively. Analogously, the signal of the DJF Niño3.4 index are also removed by the partial regression analyses. What we find is that the MAM Niño3.4 index is closely related to both the MAM and the preceding-DJF Southern Hemisphere extratropical SST. The distribution of partial regression coefficients during DJF and MAM are highly consistent, with a pattern correlation coefficient as 0.74, suggesting MAM SST anomalies related to MAM Niño3.4 index (Fig. 11d) tend to originate from the preceding DJF (Fig. 11c). The pattern correlation between Figs. 11a and c, and Figs. 11b and d, are 0.80 and 0.82, respectively, implying the SST anomaly pattern related to MAM Niño3.4 index manifests as an SOD structure. The consistency between the SOD pattern and the SST anomaly pattern related to the MAM Niño3.4 index illustrates the potential role of the SOD in influencing MAM ENSO.

Note that Fig. 11 suggests that there may be some key regions in which SST may play a stronger role in influencing MAM ENSO than in other extratropical regions. The focus of the present study is the role of the zonal-mean component, since the zonal homogeneity of the SOD is relatively clear and the SOD is indeed correlated with the DJF SAM. The correlation coefficient between the SAM and SOD is about 0.6, which is stronger than the correlation coefficients between the SAM and SST in most of specific regions in the southern extratropics, implying that the larger-scale SOD index is better at storing the SAM signal than SST anomalies in specific regions. The effect of the zonal asymmetrical component is not explored in the present study but cannot be ruled out in reality. In particular, a subtropical dipole mode is identified as the prominent mode in the Southern Hemisphere subtropical ocean, manifesting as a global wavenumber-3 subtropical dipole SST pattern and inherently existing as a thermodynamical coupled mode in the subtropical ocean–atmosphere coupled system (Wang, 2010a, 2010b). In view of these important and unique features of Southern Hemisphere SST variability, more future work is needed to understand regional differences of the Southern Hemisphere extratropical SST in influencing tropical Pacific SST.

4.2. *Influence of the MAM SOD on MAM tropical circulation*

The MAM SOD has been found to affect the MAM MMC and zonal wind from the Southern Hemisphere extratropics to the Northern Hemisphere subtropics, and has been veri-

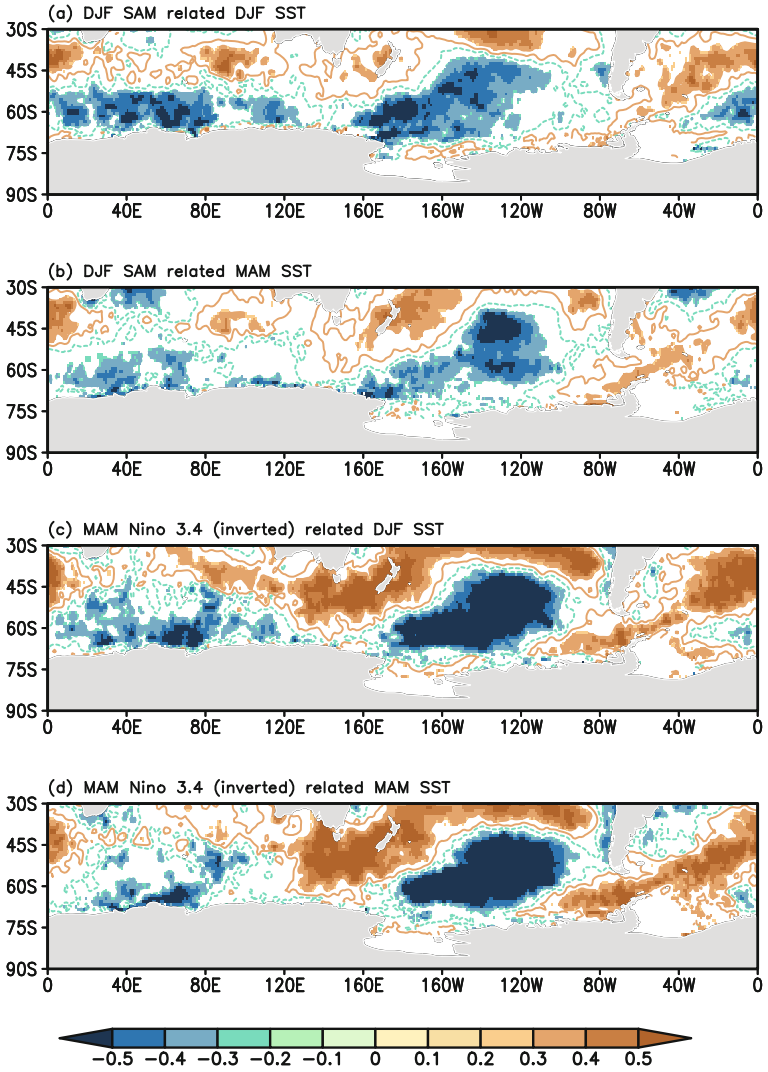

Fig. 11. Partial regression of (a, c) DJF and (b, d) MAM SST (units: °C) on the (a, b) DJF SAMI and (c, d) inverted MAM Niño3.4 index derived from reanalysis datasets. The DJF Niño3.4 signal has been removed from the DJF SAMI, MAM Niño3.4 index, and the SST field. Values not significant at the 90% confidence level are masked out by white shading. Solid (dashed) contours represent positive (negative) values.

fied using both observations and AGCM simulations (Wu et al., 2009; Zheng and Li, 2012; Zheng et al., 2015a). The partial regressions of the MAM MMC and zonal wind on the MAM SOD after removing the DJF ENSO are shown in Figs. 12a and b, respectively. An anomalous counterclockwise and clockwise circulation exist between 45°S and 30°S and south of 45°S, respectively. Besides, counterclockwise circulation occurs in the tropics (10°S–10°N) alongside anomalous descent and ascent at around 10°S and 10°N, respectively. Accordingly, it is clear in Fig. 12b that there are stronger westerlies at southern high latitudes, weaker westerlies at southern midlatitudes, anomalous westerlies in the southern subtropics, and anomalous easterlies in the tropics. Similar partial regression analyses as in Figs. 12a and b, except for regionally zonal-averaged meridional wind and zonal wind over the Pacific (100°E–60°W), are shown in Figs. 13a and b. Except for meridional circulation over the polar region (south of 60°S), the regionally zonal-averaged meridional circulation and zonal wind over the Pacific show similarity to the results of the zonal mean along the entire longitudinal circle. Specifically, easterly wind anomalies exist in the lower tropical troposphere.

A schematic diagram produced on the basis of the extratropical momentum budget, as expressed in Eq. (5), is proposed to explain the connections between the southern extratropical MMC/zonal wind and the MAM SOD (Zheng et al., 2015a). The momentum budget analysis is one effective way to understand the MMC variability. A positive MAM SOD leads to increased (decreased) baroclinicity and anomalous vertical eddy heat flux convergence (divergence) south (north) of 50°S, which is further compensated by the anomalous eddy momentum flux divergence (convergence)

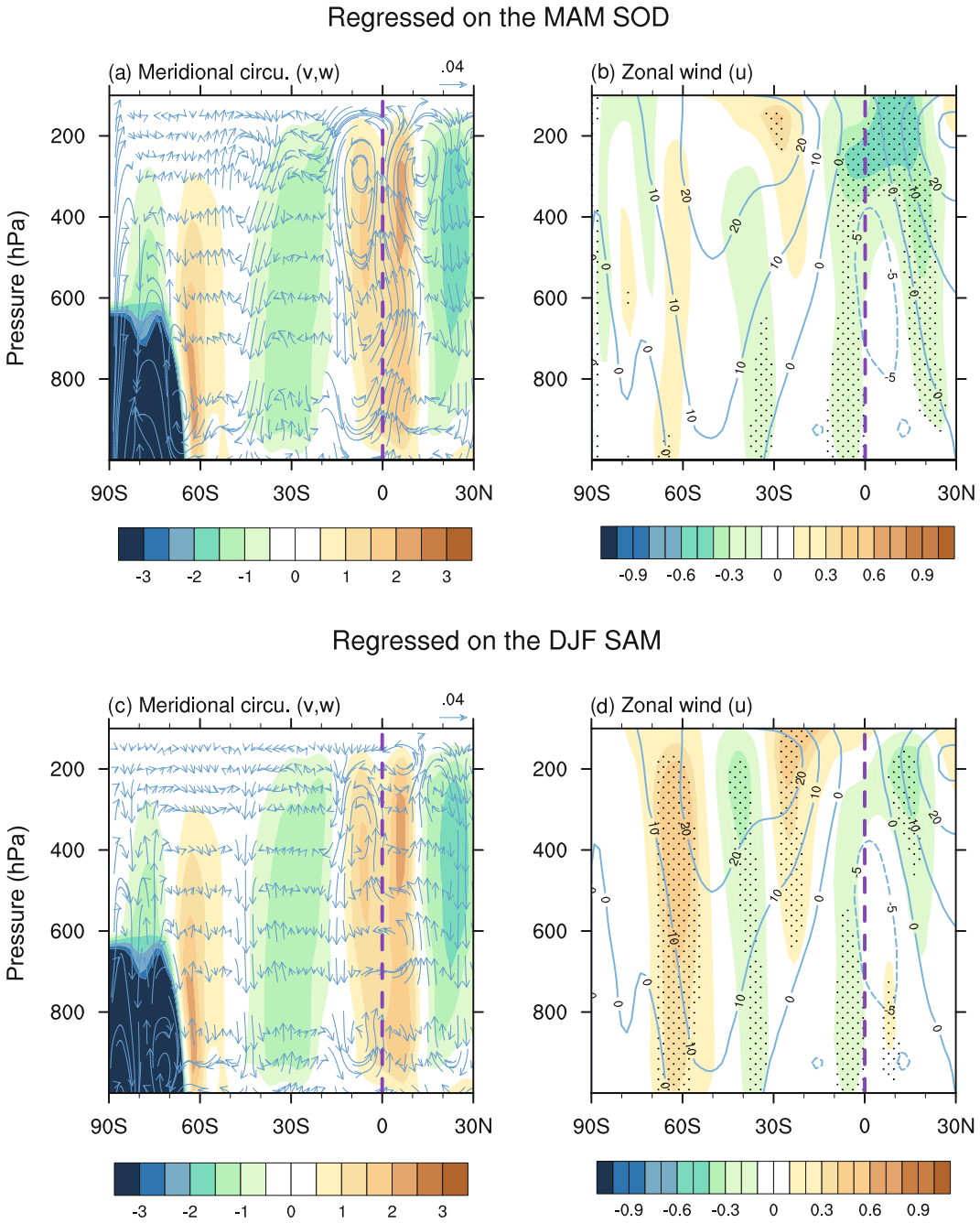

Fig. 12. Partial regression of MAM (a, c) meridional circulation (vectors) and (b, d) zonal mean wind (units: m s^{-1}; shading) on the (a, b) MAM SOD and (c, d) DJF SAMI after removing the DJF ENSO signal. In (a, c), the units for the vertical and horizontal velocity are 10^{-2} Pa s^{-1} and m s^{-1}, respectively, and the shading represents the climatological vertical velocity (units: 10^{-2} Pa s^{-1}). The blue contours in (b, d) represent the climatological mean zonal wind (units: m s^{-1}), and the stippling represents significance at the 90% confidence level. The purple dashed line indicates the position of the equator.

south (north) of 50°S. According to Eq. (5), anomalous eddy momentum flux divergence/convergence leads to anomalous northerly flow south of 50°S and anomalous southerly flow between 50°S and 30°S, thus resulting in anomalous descent and ascent at around 45°S and 30°S, respectively. Consequently, anomalous clockwise and counterclockwise cells develop in the Southern Hemisphere extratropics.

Here, we further use the momentum budget to understand the relationship between the tropical MMC and the MAM SOD. The momentum budget in the tropics is different from that in the extratropics. A comparison between Eqs. (4) and (5) shows that the momentum budget in the tropics is not only affected by divergence/convergence of eddy momentum flux, but also is determined by the meridional transport of vorticity

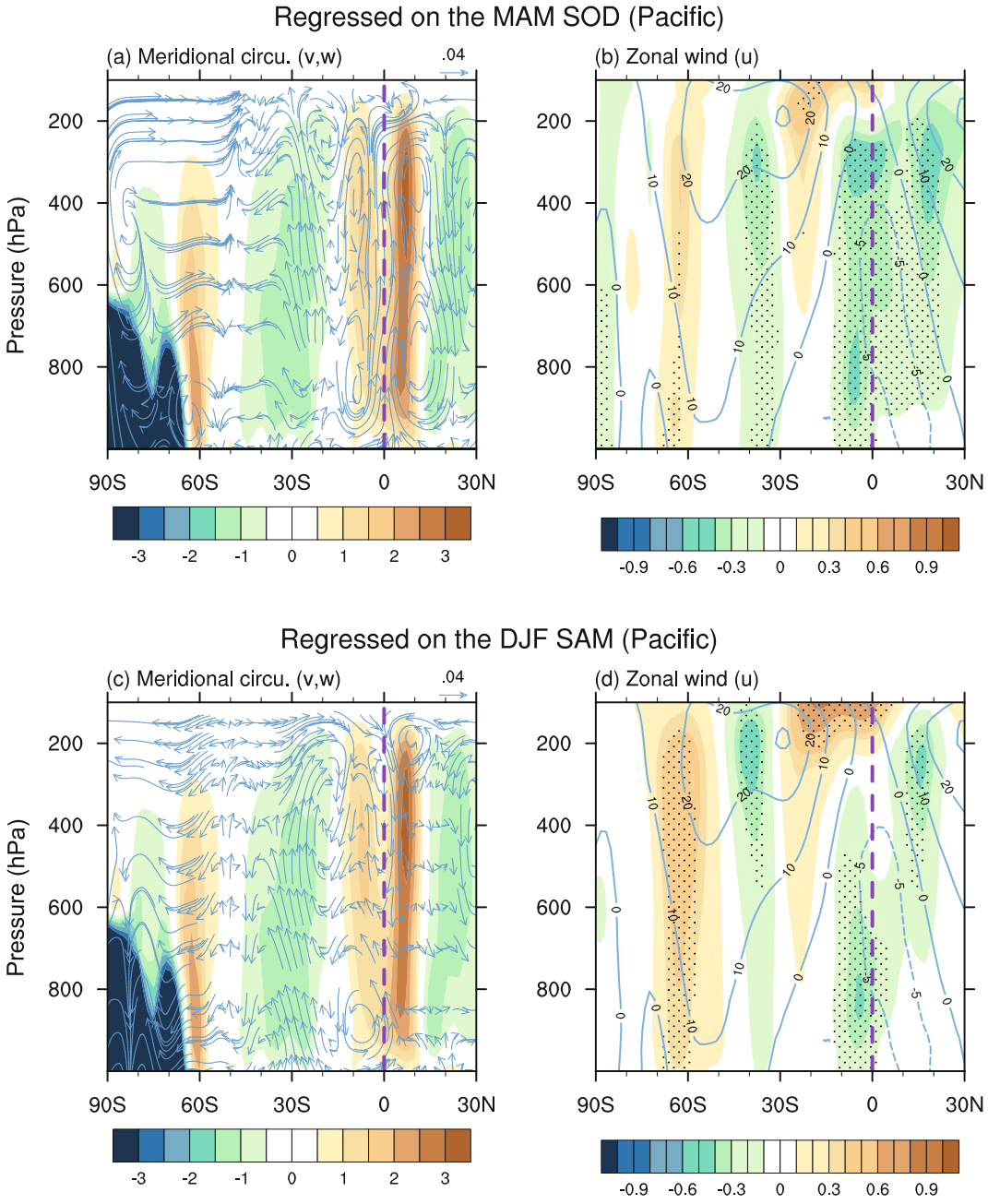

Fig. 13. As in Fig. 12, but for zonally averaged circulations over the Pacific region (100°E–60°W).

by the zonal mean flow.

Figure 14a shows the partial regression of meridional wind onto the MAM SOD after the DJF ENSO signals have been removed. There are clear northerly wind anomalies in the tropical upper troposphere (15°S–10°N), corresponding to the anomalous counterclockwise cell straddling the equator. This anomalous northerly wind indicates that the climatological poleward flow in the Northern Hemisphere tropical upper troposphere (0°–10°N) is weakened, whereas that in the Southern Hemisphere tropics (15°S–0°) is strengthened. It is known from Eq. (4) that northerly wind anomalies can be balanced by decreases in the vorticity transport term δR_o, or in the eddy stress term δS. To quantitatively explore the contributions of vorticity transport and eddy stress, the regression of the δR_o and δS terms onto the MAM SOD is shown in Figs. 14c and d, respectively. Analogously, the DJF ENSO signals have been removed by the partial regression analysis. In Fig. 14c, the δR_o term in the upper tropical (15°S–10°N) troposphere is reduced. In the Northern Hemisphere, the decreased δR_o term indicates that the poleward vorticity transport is reduced, mainly as a result of the easterly anomalies in the northern subtropics (Fig. 14b). In contrast, the reduced δR_o term in the Southern Hemisphere indicates that the poleward vorticity transport is strengthened, due mainly to the westerly anomalies in the southern subtropics. A comparison suggests that the anomalous northerly wind in the upper trop-

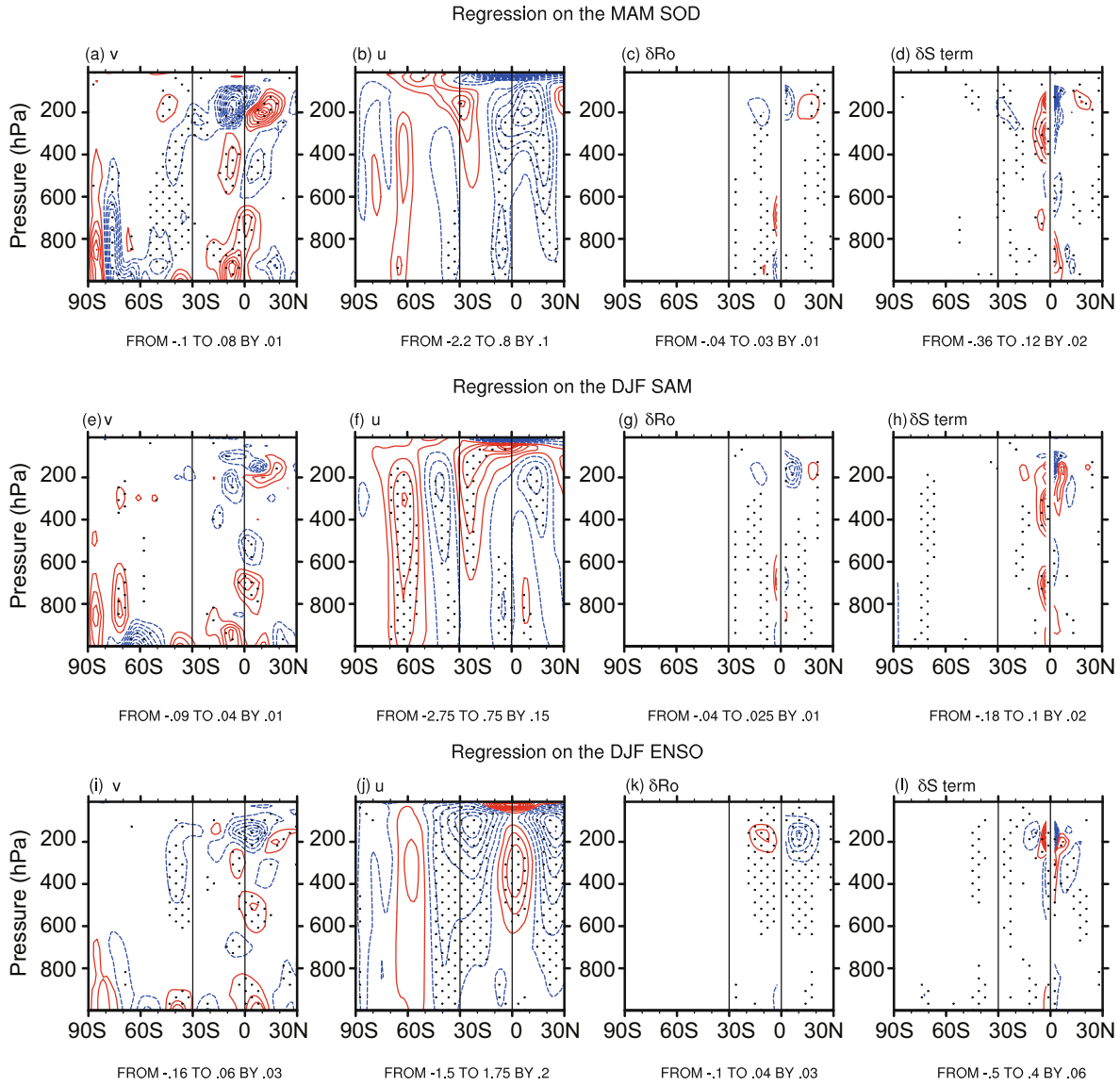

Fig. 14. Partial regression of MAM (a) meridional wind, (b) zonal wind, (c) the δR_o term, and (d) the δS term in Eq. (4) on the MAM SOD (top), DJF SAM (middle), and inverted DJF Niño3.4 index (bottom). In the top and middle panels, the DJF Niño3.4 signal has been removed by partial regression. In the bottom panels, the DJF SAM signal has been removed. The contour intervals are labeled at the bottom of each panel, and the units are m s^{-1}. Stippling represents significance at the 90% confidence level. The blue (red) contours represent negative (positive) values.

ical troposphere is mainly balanced by the reductions in the δR_o term. The eddy stress generally plays a secondary role in balancing the northerly wind anomalies in the upper tropical troposphere, compensating in part for the reduced δR_o term.

Similar regression analyses as in Figs. 12a and b, Figs. 13a and b, and Figs. 14a–d are conducted for the DJF SAM, and the results are shown in Figs. 12c and d, Figs. 13c and d, and Figs. 14e–h. The regression patterns are generally in agreement with those regressed on the MAM SOD. The consistency suggests again that a bridging role of the MAM SOD in the influence of the DJF SAM on MAM ENSO.

Furthermore, to clearly show the differences between the DJF SAM and DJF ENSO from the aspect of influencing the MAM MMC/zonal wind, a similar analysis to Figs. 14a–d is provided for the DJF ENSO, the results of which are shown in Figs. 14i–l. The SAM signal is linearly excluded in the analysis for ENSO to detect the influence of ENSO without SAM variability. In view of the negative correlation between ENSO and the SAM, the Niño3.4 index is inverted to enable a more convenient comparison with the SAM.

The meridional wind regressed onto the DJF ENSO is shown in Fig. 14i. A cursory comparison of Figs. 14i and e suggests that the anomalous meridional wind associated with the DJF ENSO and DJF SAM show some degree of similarity. Northerly wind anomalies exist in the tropical upper troposphere. An obvious difference between the SAM-related and ENSO-related tropical circulation anomalies emerges in the subtropical zonal wind, as shown in Figs. 14f and j. The

ENSO-related zonal wind anomalies are strongly symmetric about the equator. The subtropical westerlies in the two hemispheres both weaken (strengthen) corresponding to the cold (warm) phase of ENSO. In contrast, the SAM-related zonal wind anomalies in the tropics show a degree of equatorial asymmetry, with strengthened westerlies in the Southern Hemisphere subtropics and weakened westerlies in the Northern Hemisphere subtropics.

Figure 14k shows that the δR_o term reduces in the northern tropics (0°–10°N), but increases in the southern tropics (10°S–0°). Therefore, the δR_o term in the northern tropics (0°–10°N) makes a same-sign contribution to the anomalous northerly wind in the upper tropical troposphere, which is similar to the case for the SAM (Fig. 14g). However, the δR_o term in the southern tropics (10°S–0°) makes an opposite-sign contribution to the anomalous northerly wind, which is opposite to the case for the SAM. The anomalous northerly wind in the upper tropical troposphere in the southern tropics (10°S–0°) is mainly balanced by changes in the eddy stress. The momentum budget in the Southern Hemisphere tropics for the ENSO case is markedly different to the SOD case.

In short, although the DJF SAM- and DJF ENSO-related tropical circulations in MAM have some common features, significant differences also exist. Especially in the Southern Hemisphere tropics (10°S–0°), the roles of vorticity transport (the δR_o term) are totally different, mainly due to differences in Southern Hemisphere subtropical westerlies related to the SAM and ENSO. Therefore, although the DJF SAM and DJF ENSO are closely linked, their influence on the MAM tropical MMC/zonal wind and the corresponding mechanisms are different, which provides further evidence that the influence of the DJF SAM on the MAM tropical circulation is not simply a reflection of DJF ENSO variability.

4.3. *Tropical coupled responses*

The composite differences in atmospheric circulation over the tropical Pacific during MAM between the high and low MAM SOD years are shown in Fig. 15a, which refer to years with SOD index more (less) than one standard deviation above (below) the mean during the period 1950/51–2015/16. To exclude ENSO effects, the composite analyses are carried out after filtering out the typical ENSO years, as illustrated in section 3.3. As shown in Fig. 15a, anomalous easterly winds occur over the equatorial Pacific, implying that MAM trade winds in that region are enhanced (reduced) when the MAM SOD is in a positive (negative) phase. A pair of anticyclonic circulation anomalies occurs on the south and north sides of the anomalous easterly wind over the central tropical Pacific.

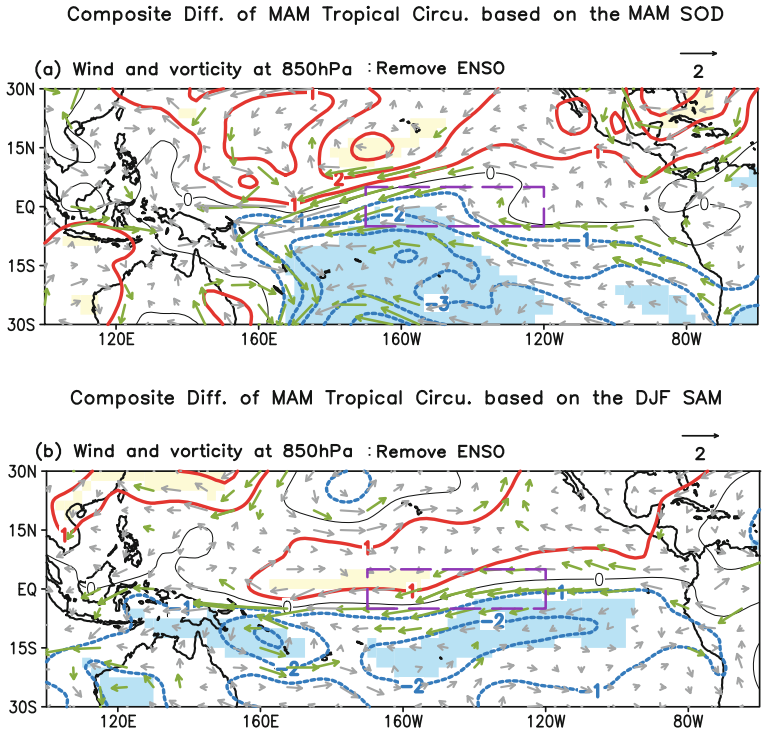

Fig. 15. (a) Composite difference in MAM horizontal wind (arrows; units: m s^{-1}) and vorticity (contours; 10^6 m^2 s^{-1}) at 850 hPa between high and low MAM SOD years. The definitions of the high and low SOD years are described in section 4.3. Typical ENSO years have been excluded when calculating the composite differences. The shading and green vectors represent significance at the 90% confidence level. The Niño3.4 region is indicated by the purple dashed box. (b) As in (a), but for the composite difference between the high and low DJF SAM years.

Similar composite analyses as in Fig. 15a are conducted for the DJF SAM, and the results are shown in Fig. 15b. A large-scale agreement exists between Figs. 15a and b, suggesting a role of the MAM SOD in the influence of the DJF SAM on MAM circulation.

The above circulation anomalies are associated with positive Bjerkness feedback (Bjerknes, 1969) in the tropics, in which easterly surface wind stress enhances cooler SST, which in turns amplifies wind stress. Consequently, perturbation of the atmospheric circulation and SST anomalies in association with the DJF SAM are amplified by the Bjerkness feedback, thus causing a cooler (warmer) MAM SST in the central tropical Pacific when the DJF SAM is in a positive (negative) phase.

5. Discussion and conclusions

ENSO has a remarkable influence on global climate, and considerable effort has been devoted to detecting the factors that influence ENSO. Despite the large consensus in the literature regarding the fundamental role that the interaction between the atmosphere and ocean in the tropical Pacific plays in determining the characteristics of ENSO, there is growing evidence for the role of extratropical forcings in triggering ENSO events or influencing the amplitude of ENSO. This paper investigates the influence of the DJF SAM on the amplitude of ENSO decay during MAM, and sheds additional light on extratropical forcings of ENSO.

This study highlights the influence of the DJF SAM on MAM SST over the Niño3.4 region. The mechanisms associated with this influence can be briefly summarized as follows: The SAM is positively correlated with SST at southern high latitudes, but negatively correlated in the southern midlatitudes. Dipole-like SST anomalies caused by the SAM are referred to as the SOD. The DJF SAM-induced DJF SOD can persist until MAM, and then influence the MAM MMC and zonal wind. Specifically, a positive (negative) DJF SAM commonly results in a positive (negative) phase of the MAM SOD, which tends to strengthen (weaken) trade winds in the central tropical Pacific. Strengthened (weakened) trade wind anomalies produce cooler (warmer) SST. Accordingly, anomalous trade winds and SST related to the DJF SAM further sustain and develop via Bjerkness feedback, which eventually results in a cooling (warming) in the central tropical Pacific. Specifically, El Niño-like warm SST anomalies over the central Pacific during MAM corresponding to the positive DJF SAM are weaker than those corresponding to the negative DJF SAM; meanwhile, La Niña-like cooler SST anomalies over the central Pacific during MAM corresponding to the positive DJF SAM are stronger than those corresponding to the negative DJF SAM.

Previous studies have found that Southern Hemisphere extratropical SSTs can regulate ENSO activity (Terray, 2011; Zhang et al., 2014a, 2014b; Ding et al., 2015; Yamazaki and Watanabe, 2015) through processes such as the propagation of subtropical SST anomalies (Zhang et al., 2014a, 2014b; Ding et al., 2015) into the tropics or energy transport caused by extratropical warming (Yamazaki and Watanabe, 2015). This study provides further evidence for the influences of the Southern Hemisphere extratropical SST on ENSO through the responses of the MMC and subsequent coupled air–sea responses in the tropics. Yamazaki and Watanabe (2015) also pointed out responses of the Hadley cell to Southern Hemisphere extratropical SST (see also Chiang and Bitz, 2005; Kang et al., 2008). Note that SST anomalies are uniformly warm south of 30°S in Yamazaki and Watanabe (2015). However, SST anomalies in this study exhibit a dipole-like structure, with warmer (colder) SST in the midlatitudes but colder (warmer) SST in the high latitudes, and vice versa. The focus of the present study is the role of the zonal-mean component of Southern Hemisphere extratropical SST. There are several clues in this study to suggest there may be some key regions in which SST plays a stronger role in influencing the amplitude of MAM ENSO than in other extratropical regions. More work is needed in the future to understand the regional differences in the influence of Southern Hemisphere extratropical SST on tropical Pacific SST.

Acknowledgements. The authors would like to thank the editor and the anonymous reviewers for their insightful comments and suggestions, which contributed greatly towards improving the manuscript. This work was jointly supported by the China Special Fund for Meteorological Research in the Public Interest (Grant No. GYHY201506032), an NSFC project (Grant No. 41405086), and a National Key R&D Program of China (Grant No. 2016YFA0601801). The datasets, including NCEP–NCAR, 20CR, CMAP, GPCP, and ERSST.v3b, were obtained from NOAA/OAR/ESRL PSD, Boulder, Colorado, USA, via their website: http://www.esrl.noaa.gov/psd/. The HadISST dataset was provided by the Met Office Hadley Centre. We acknowledge the World Climate Research Programme's Working Group on Coupled Modelling, which is responsible for CMIP, and we thank the climate modeling groups for producing and making available their model output.

REFERENCES

Baldwin, M. P., 2001: Annular modes in global daily surface pressure. *Geophys. Res. Lett.*, **28**, 4115–4118, doi: 10.1029/2001GL013564.

Bjerknes, J., 1969: Atmospheric teleconnections from the equatorial Pacific. *Mon. Wea. Rev.*, **97**, 163–172, doi: 10.1175/1520-0493(1969)097<0163:ATFTEP>2.3.CO;2.

Caballero, R., 2007: Role of eddies in the interannual variability of Hadley cell strength. *Geophys. Res. Lett.*, **34**, L22705, doi: 10.1029/2007GL030971.

Cai, W. J., and I. G. Watterson, 2002: Modes of interannual variability of the Southern Hemisphere circulation simulated by the CSIRO climate model. *J. Climate*, **15**, 1159–1174, doi: 10.1175/1520-0442(2002)015<1159:MOIVOT>2.0.CO;2.

Chen, S. F., B. Yu, and W. Chen, 2014: An analysis on the physical process of the influence of AO on ENSO. *Climate Dyn.*, **42**, 973–989, doi: 10.1007/s00382-012-1654-z.

Chiang, J. C. H., and D. J. Vimont, 2004: Analogous Pacific and Atlantic meridional modes of tropical atmosphere–ocean variability. *J. Climate*, **17**, 4143–4158, doi: 10.1175/JCLI

4953.1.

Chiang, J. C. H., and C. M. Bitz, 2005: Influence of high latitude ice cover on the marine intertropical convergence zone. *Climatic Dyn*., **25**, 477–496, doi: 10.1007/s00382-005-0040-5.

Ciasto, L. M., G. R. Simpkins, and M. H. England, 2015: Teleconnections between tropical pacific SST anomalies and extratropical southern hemisphere climate. *J. Climate*, **28**, 56–65, doi: 10.1175/JCLI-D-14-00438.1.

Compo, G. P., and P. D. Sardeshmukh, 2010: Removing ENSO-related variations from the climate record. *J. Climate*, **23**, 1957–1978, doi: 10.1175/2009JCLI2735.1.

Deser, C., M. A. Alexander, and M. S. Timlin, 2003: Understanding the persistence of sea surface temperature anomalies in midlatitudes. *J. Climate*, **16**, 57–72, doi: 10.1175/1520-0442(2003)016<0057:UTPOSS>2.0.CO;2.

Deser, C., M. A. Alexander, S.-P. Xie, and A. S. Phillips, 2010: Sea surface temperature variability: patterns and mechanisms. *Annual Review of Marine Science*, **2**, 115–143, doi: 10.1146/annurev-marine-120408-151453.

Ding, R. Q., J. P. Li, and Y. H. Tseng, 2015: The impact of South Pacific extratropical forcing on ENSO and comparisons with the North Pacific. *Climate Dyn*., **44**, 2017–2034, doi: 10.1007/s00382-014-2303-5.

Ding, Q. H., E. J. Steig, D. S. Battisti, and J. M. Wallace, 2012: Influence of the tropics on the Southern Annular Mode. *J. Climate*, **25**, 6330–6348, doi: 10.1175/JCLI-D-11-00523.1.

Dommenget, D., 2010: The slab ocean El Niño. *Geophys. Res. Lett*., **37**, L20701, doi: 10.1029/2010GL044888.

Feldstein, S. B., and S. Lee, 1998: Is the atmospheric zonal index driven by an eddy feedback? *J. Atmos. Sci*., **55**, 3077–3086, doi: 10.1175/1520-0469(1998)055<3077:ITAZID>2.0.CO;2.

Feng, J., and J. P. Li, 2011: Influence of El Niño Modoki on spring rainfall over South China. *J. Geophys. Res*., **116**(D13), D13102, doi: 10.1029/2010JD015160.

Fogt, R. L., and D. H. Bromwich, 2006: Decadal variability of the ENSO teleconnection to the high-latitude South Pacific governed by coupling with the Southern annular mode. *J. Climate*, **19**, 979–997, doi: 10.1175/JCLI3671.1.

Fogt, R. L., J. Perlwitz, A. J. Monaghan, D. H. Bromwich, J. M. Jones, and G. J. Marshall, 2009a: Historical SAM variability. Part II: Twentieth-century variability and trends from reconstructions, observations, and the IPCC AR4 models. *J. Climate*, **22**, 5346–5365, doi: 10.1175/2009JCLI2786.1.

Gillett, N. P., and D. W. J. Thompson, 2003: Simulation of recent Southern Hemisphere climate change. *Science*, **302**, 273–275, doi: 10.1126/science.1087440.

Gong, D. Y., and S. W. Wang, 1999: Definition of Antarctic oscillation index. *Geophys. Res. Lett*., **26**, 459–462, doi: 10.1029/1999GL900003.

Gong, T. T., S. B. Feldstein, and D. H. Luo, 2010: The impact of ENSO on wave breaking and Southern annular mode events. *J. Atmos. Sci*., **67**, 2854–2870, doi: 10.1175/2010JAS3311.1.

Gupta, A. S., and M. H. England, 2006: Coupled ocean–atmosphere–ice response to variations in the Southern Annular Mode. *J. Climate*, **19**, 4457–4486, doi: 10.1175/JCLI3843.1.

Gupta, A. S., and M. H. England, 2007: Coupled ocean-atmosphere feedback in the southern annular mode. *J. Climate*, **20**, 3677–3692, doi: 10.1175/JCLI4200.1.

Hamlington, B. D., R. F. Milliff, H. van Loon, and K.-Y. Kim, 2015: A Southern Hemisphere sea level pressure-based precursor for ENSO warm and cold events. *J. Geophys. Res*., **120**, 2280–2292, doi: 10.1002/2014JD022674.

Hartmann, D. L., and F. Lo, 1998: Wave-driven zonal flow vacillation in the Southern Hemisphere. *J. Atmos. Sci*., **55**, 1303–1315, doi: 10.1175/1520-0469(1998)055<1303:WDZFVI>2.0.CO;2.

Hong, L. C., LinHo, and F. F. Jin, 2014: A southern hemisphere booster of super El Niño. *Geophys. Res. Lett*., **41**, 2142–2149, doi: 10.1002/2014GL059370.

Jin, F.-F., 1997: An equatorial ocean recharge paradigm for ENSO. Part I: Conceptual model. *J. Atmos. Sci*., **54**, 811–829, doi: 10.1175/1520-0469(1997)054<0811:AEORPF>2.0.CO;2.

Kalnay, E., and Coauthors, 1996: The NCEP/NCAR 40-year reanalysis project. *Bull. Amer. Meteor. Soc*., **77**, 437–470, doi: 10.1175/1520-0477(1996)077<0437:TNYRP>2.0.CO;2.

Kang, S. M., and J. Lu, 2012: Expansion of the Hadley Cell under global warming: Winter versus summer. *J. Climate*, **25**, 8387–8393, doi: 10.1175/JCLI-D-12-00323.1.

Kang, S. M., I. M. Held, D. M. W. Frierson, and M. Zhao, 2008: The response of the ITCZ to extratropical thermal forcing: Idealized slab-ocean experiments with a GCM. *J. Climate*, **21**, 3521–3532, doi: 10.1175/2007JCLI2146.1.

Kang, S. M., L. M. Polvani, J. C. Fyfe, and M. Sigmond, 2011: Impact of polar ozone depletion on subtropical precipitation. *Science*, **332**, 951–954, doi: 10.1126/science.1202131.

L'Heureux, M. L., and D. W. J. Thompson, 2006: Observed relationships between the El Niño–Southern Oscillation and the extratropical zonal-mean circulation. *J. Climate*, **19**, 276–287, doi: 10.1175/JCLI3617.1.

Larson, S., and B. Kirtman, 2013: The pacific meridional mode as a trigger for ENSO in a high-resolution coupled model. *Geophys. Res. Lett*., **40**, 3189–3194, doi: 10.1002/grl.50571.

Larson, S. M., and B. P. Kirtman, 2014: The pacific meridional mode as an ENSO precursor and predictor in the North American multimodel ensemble. *J. Climate*, **27**, 7018–7032, doi: 10.1175/JCLI-D-14-00055.1.

Latif, M., and Coauthors, 1998: A review of the predictability and prediction of ENSO. *J. Geophys. Res*., **103**(C7), 14 375–14 393, doi: 10.1029/97JC03413.

Lefebvre, W., H. Goosse, R. Timmermann, and T. Fichefet, 2004: Influence of the southern annular mode on the sea ice–ocean system. *J. Geophys. Res*., **109**(C9), 2004, doi: 10.1029/2004JC002403.

Li, J. P., 2016: Impacts of annular modes on extreme climate events over the East Asian Monsoon region. *Dynamics and Predictability of Large-Scale*, *High-Impact Weather and Climate Events*, J. P. Li, R. Swinbank, R. Grotjahn, and H. Volkert, Eds., Cambridge University Press.

Li, J. P., and J. X. L. Wang, 2003: A modified zonal index and its physical sense. *Geophys. Res. Lett*., **30**, 1632, doi: 10.1029/2003GL017441.

Li, J. P., and Coauthors, 2013: Progress in air–land–sea interactions in Asia and their role in global and Asian climate change. *Chinese Journal of Atmospheric Sciences*, **37**, 518–538, doi: 10.3878/j.issn.1006-9895.2012.12322. (in Chinese)

Liu, T., J. P. Li, and F. Zheng, 2015: Influence of the boreal autumn southern annular mode on winter precipitation over land in the northern hemisphere. *J. Climate*, **28**, 8825–8839, doi: 10.1175/JCLI-D-14-00704.1.

Lorenz, D. J., and D. L. Hartmann, 2001: Eddy–zonal flow feedback in the southern hemisphere. *J. Atmos. Sci*., **58**, 3312–3327, doi: 10.1175/1520-0469(2001)058<3312:EZFFIT>2.

0.CO;2.

Luo, D. H., A. R. Lupo, and H. Wan, 2007: Dynamics of eddy-driven low-frequency dipole modes. Part I: A simple model of North Atlantic oscillations. *J. Atmos. Sci*., **64**, 3–28, doi: 10.1175/JAS3818.1.

Marshall, G. J., 2003: Trends in the southern annular mode from observations and reanalyses. *J. Climate*, **16**, 4134–4143, doi: 10.1175/1520-0442(2003)016<4134:TITSAM>2.0.CO;2.

Nan, S. L., and J. P. Li, 2003: The relationship between the summer precipitation in the Yangtze River valley and the boreal spring southern hemisphere annular mode. *Geophys. Res. Lett*., **30**, 2266, doi: 10.1029/2003GL018381.

Shi, W. J., Z. N. Xiao, and J. J. Xue, 2016: Teleconnected influence of the boreal winter Antarctic Oscillation on the Somali Jet: Bridging role of sea surface temperature in southern high and middle latitudes. *Adv. Atmos. Sci.*, **33**, 47–57, doi: 10.1007/s00376-015-5094-7.

Terray, P., 2011: Southern Hemisphere extra-tropical forcing: A new paradigm for El Niño-Southern Oscillation. *Climate Dyn*., **36**, 2171–2199, doi: 10.1007/s00382-010-0825-z.

Thompson, D. W. J., and J. M. Wallace, 2000: Annular modes in the extratropical circulation. Part I: Month-to-month variability. *J. Climate*, **13**, 1000–1016, doi: 10.1175/1520-0442(2000)013<1000:AMITEC>2.0.CO;2.

Thompson, D. W. J., and D. J. Lorenz, 2004: The signature of the annular modes in the tropical troposphere. *J. Climate*, **17**, 4330–4342, doi: 10.1175/3193.1.

Thompson, D. W. J., S. Solomon, P. J. Kushner, M. H. England, K. M. Grise, and D. J. Karoly, 2011: Signatures of the Antarctic ozone hole in Southern Hemisphere surface climate change. *Nat. Geosci.*, **4**, 741–749, doi: 10.1038/ngeo1296.

van Loon, H., and D. J. Shea, 1985: The Southern Oscillation. Part IV: The precursors south of 15°S to the extremes of the oscillation. *Mon. Wea. Rev*., **113**, 2063–2074, doi: 10.1175/1520-0493(1985)113<2063:TSOPIT>2.0.CO;2.

Vimont D. J., D. S. Battisti, and A. C. Hirst, 2001: Footprinting: A seasonal connection between the tropics and mid-latitudes. *Geophys. Res. Lett*., **28**, 3923–3926, doi: 10.1029/2001GL013435.

Vimont, D. J., J. M. Wallace, and D. S. Battisti, 2003: The seasonal footprinting mechanism in the Pacific: Implications for ENSO. *J. Climate*, **16**, 2668–2675, doi: 10.1175/1520-0442(2003)016<2668:TSFMIT>2.0.CO;2.

Walker, C. C., and T. Schneider, 2006: Eddy influences on Hadley circulations: Simulations with an idealized GCM. *J. Atmos. Sci*., **63**, 3333–3350, doi: 10.1175/JAS3821.1.

Wang, B., R. G. Wu, and X. H. Fu, 2000: Pacific–East Asian teleconnection: How does ENSO affect East Asian climate? *J. Climate*, **13**, 1517–1536, doi: 10.1175/1520-0442(2000)013<1517:PEATHD>2.0.CO;2.

Wang, F., 2010a: Subtropical dipole mode in the Southern Hemisphere: A global view. *Geophys. Res. Lett*., **37**, L10702, doi: 10.1029/2010GL042750.

Wang, F. M., 2010b: Thermodynamic coupled modes in the tropical atmosphere-ocean: An analytical solution. *J. Atmos. Sci*., **67**, 1667–1677, doi: 10.1175/2009JAS3262.1.

Wang, S.-Y., M. L. L'Heureux, and H. H. Chia, 2012a: ENSO prediction one year in advance using western North Pacific sea surface temperatures. *Geophys. Res. Lett*., **39**, L05702, doi: 10.1029/2012GL050909.

Wang, S. Y., M. L'Heureux, and J. H. Yoon, 2012b: Is global warming changing the ENSO precursor in the western north pacific? *37th NOAA Annual Climate Diagnostics and Prediction Workshop*, Fort Collins, CO, NOAA, 115–120.

Watanabe, M., and A. T. Wittenberg, 2012: A method for disentangling El Niño-mean state interaction. *Geophys. Res. Lett*., **39**, L14702, doi: 10.1029/2012GL052013.

Watterson, I. G., 2000: Southern midlatitude zonal wind vacillation and its interaction with the ocean in GCM simulations. *J. Climate*, **13**, 562–578, doi: 10.1175/1520-0442(2000)013<0562:SMZWVA>2.0.CO;2.

Wu, Z. W., J. P. Li, B. Wang, and X. H. Liu, 2009: Can the Southern Hemisphere annular mode affect China winter monsoon? *J. Geophys. Res*., **114**(D11), D11107, doi: 10.1029/2008JD011501.

Xie, S. P., 2004: Satellite observations of cool ocean–atmosphere interaction. *Bull. Amer. Meteor. Soc*., **85**, 195–208, doi: 10.1175/BAMS-85-2-195.

Yamazaki, K., and M. Watanabe, 2015: Effects of extratropical warming on ENSO amplitudes in an ensemble of a coupled GCM. *Climate Dyn*., **44**, 679–693, doi: 10.1007/s00382-014-2145-1.

Zhang, H. H, A. Clement, and P. Di Nezio, 2014a: The south pacific meridional mode: A mechanism for ENSO-like variability. *J. Climate*, **27**, 769–783, doi: 10.1175/JCLI-D-13-00082.1.

Zhang, H. H., A. Clement, and B. Medeiros, 2016: The meridional mode in an idealized aquaplanet model: Dependence on the mean state. *J. Climate*, **29**, 2889–2905, doi: 10.1175/JCLI-D-15-0399.1.

Zhang, Y., X. Q. Yang, Y. Nie, and G. Chen, 2012: Annular mode-like variation in a multilayer quasigeostrophic model. *J. Atmos. Sci*., **69**, 2940–2958, doi: 10.1175/JAS-D-11-0214.1.

Zhang, H. H., C. Deser, A. Clement, and R. Tomas, 2014b: Equatorial signatures of the pacific meridional modes: Dependence on mean climate state. *Geophys. Res. Lett*., **41**, 568–574, doi: 10.1002/2013GL058842.

Zheng, F., and J. P. Li, 2012: Impact of preceding boreal winter southern hemisphere annular mode on spring precipitation over south China and related mechanism. *Chinese Journal of Geophysics*, **55**, 3542–3557, doi: 10.6038/j.issn.0001-5733.2012.11.004. (in Chinese)

Zheng, F., J. P. Li, L. Wang, F. Xie, and X. F. Li, 2015a: Cross-seasonal influence of the December–February southern hemisphere annular mode on March–May meridional circulation and precipitation. *J. Climate*, **28**, 6859–6881, doi: 10.1175/JCLI-D-14-00515.1.

Zheng, F., J. P. Li, J. Feng, Y. J. Li, and Y. Li, 2015b: Relative importance of the austral summer and autumn SAM in modulating southern hemisphere extratropical autumn SST. *J. Climate*, **28**, 8003–8020, doi: 10.1175/JCLI-D-15-0170.1.

Zhou, T. J., and R. C. Yu, 2004: Sea-surface temperature induced variability of the Southern Annular Mode in an atmospheric general circulation model. *Geophys. Res. Lett*., **31**, L24206, doi: 10.1029/2004GL021473.